Article

Cell Reports

HILPDA Uncouples Lipid Droplet Accumulation in Adipose Tissue Macrophages from Inflammation and Metabolic Dysregulation

Graphical Abstract

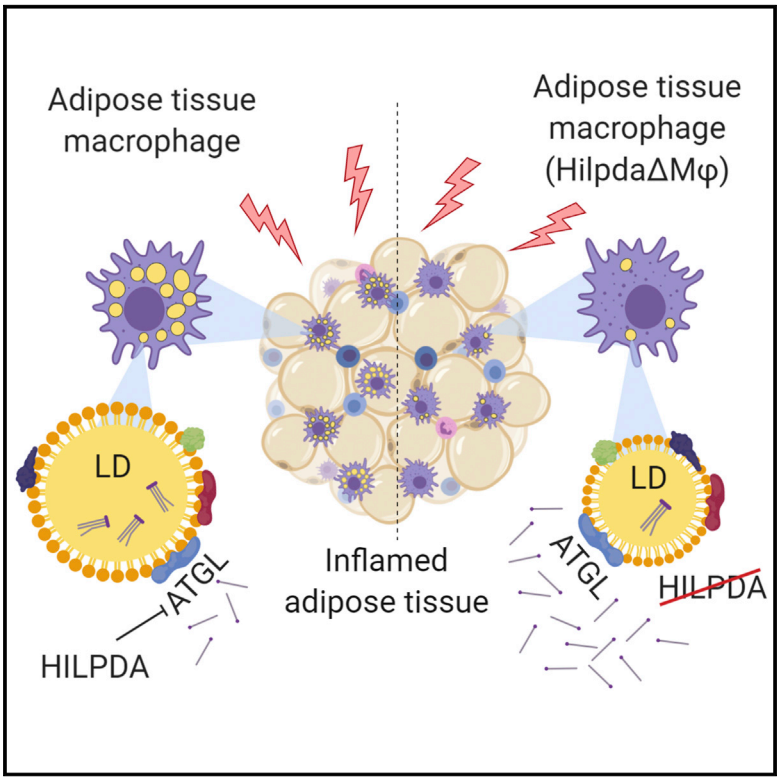

Highlights

- HILPDA is a lipid-induced, physiological inhibitor of ATGL-mediated lipolysis
- HILPDA-deficient macrophages show enhanced breakdown of triglycerides through ATGL
- Reduced lipid storage in macrophages does not affect adipose tissue inflammation

Authors

Xanthe A.M.H. van Dierendonck, Montserrat A. de la Rosa Rodriguez, Anastasia Georgiadi, ..., Jan Willem Borst, Rinke Stienstra, Sander Kersten

Correspondence

rinke.stienstra@wur.nl (R.S.), sander.kersten@wur.nl (S.K.)

In Brief

Lipid-laden macrophages are believed to play a key role in obesity-induced adipose tissue inflammation. Van Dierendonck et al. show that the lipid-droplet-associated protein HILPDA regulates intracellular triglyceride breakdown by directly inhibiting ATGL and that reduced lipid accumulation in adipose tissue macrophages surprisingly does not affect adipose tissue inflammation.

van Dierendonck et al., 2020, Cell Reports *30*, 1811–1822
February 11, 2020
https://doi.org/10.1016/j.celrep.2020.01.046

CellPress

Cell Reports
Article

HILPDA Uncouples Lipid Droplet Accumulation in Adipose Tissue Macrophages from Inflammation and Metabolic Dysregulation

Xanthe A.M.H. van Dierendonck,[1,2,9] Montserrat A. de la Rosa Rodriguez,[1,9] Anastasia Georgiadi,[1,7] Frits Mattijssen,[1] Wieneke Dijk,[1,8] Michel van Weeghel,[3,4] Rajat Singh,[5] Jan Willem Borst,[6] Rinke Stienstra,[1,2,10,*] and Sander Kersten[1,10,11,*]
[1]Nutrition, Metabolism and Genomics Group, Division of Human Nutrition and Health, Wageningen University, Stippeneng 4, 6708 WE Wageningen, the Netherlands
[2]Department of Internal Medicine, Radboud University Medical Center, Geert Grooteplein 8, 6525 GA Nijmegen, the Netherlands
[3]Laboratory Genetic Metabolic Diseases, Amsterdam UMC, University of Amsterdam, Meibergdreef 9, 1105 AZ Amsterdam, the Netherlands
[4]Gastroenterology and Metabolism, Amsterdam Cardiovascular Sciences, Meibergdreef 9, 1105 AZ Amsterdam, the Netherlands
[5]Department of Medicine, Albert Einstein College of Medicine, 1300 Morris Park Avenue, Forchheimer 505D, Bronx, NY 10461, USA
[6]Laboratory of Biochemistry, Microspectroscopy Research Facility, Wageningen University, Stippeneng 4, 6708 WE Wageningen, the Netherlands
[7]Present address: Institute for Diabetes and Cancer (IDC), Helmholtz Zentrum München, German Research Center for Environmental Health, Ingolstädter Landstraße 1, 85764 Neuherberg, Germany
[8]Present address: L'Institut du Thorax, U1087, INSERM, Nantes, France
[9]These authors contributed equally
[10]Senior author
[11]Lead Contact
*Correspondence: rinke.stienstra@wur.nl (R.S.), sander.kersten@wur.nl (S.K.)
https://doi.org/10.1016/j.celrep.2020.01.046

SUMMARY

Obesity leads to a state of chronic, low-grade inflammation that features the accumulation of lipid-laden macrophages in adipose tissue. Here, we determined the role of macrophage lipid-droplet accumulation in the development of obesity-induced adipose-tissue inflammation, using mice with myeloid-specific deficiency of the lipid-inducible HILPDA protein. HILPDA deficiency markedly reduced intracellular lipid levels and accumulation of fluorescently labeled fatty acids. Decreased lipid storage in HILPDA-deficient macrophages can be rescued by inhibition of adipose triglyceride lipase (ATGL) and is associated with increased oxidative metabolism. In diet-induced obese mice, HILPDA deficiency does not alter inflammatory and metabolic parameters, despite markedly reducing lipid accumulation in macrophages. Overall, we find that HILPDA is a lipid-inducible, physiological inhibitor of ATGL-mediated lipolysis in macrophages and uncouples lipid storage in adipose tissue macrophages from inflammation and metabolic dysregulation. Our data question the contribution of lipid droplet accumulation in adipose tissue macrophages in obesity-induced inflammation and metabolic dysregulation.

INTRODUCTION

The prevalence of obesity across the world has risen steeply in the past decades and has become a huge public health concern. It is well established that obesity is associated with a state of chronic, low-grade inflammation. That low-grade inflammation is characterized by increased production of several inflammatory cytokines and adipokines and has been suggested to be an important pathophysiological mechanism underlying many of the adverse health effects of obesity (Gregor and Hotamisligil, 2011). In particular, the increase in inflammatory cytokines and adipokines is believed to disrupt insulin signaling and to contribute to obesity-induced insulin resistance (Hotamisligil, 2017).

Adipose tissue mainly consists of adipocytes, but it also harbors numerous immune cells, including macrophages. Those macrophages are important for maintaining homeostasis in healthy adipose tissue but also contribute to the development of inflammation during obesity (Boutens and Stienstra, 2016). In lean states, adipose tissue macrophages mainly show anti-inflammatory phenotypes and are distributed evenly throughout the adipose tissue. In contrast, in obese adipose tissue, macrophages accumulate in so-called crown-like structures around dead adipocytes and display a metabolically activated phenotype (Cinti et al., 2005; Lumeng et al., 2007; Xu et al., 2013). Metabolically activated macrophages form multiple intracellular lipid droplets and display distinct transcriptional profiles (Lumeng et al., 2008; Shapiro et al., 2013; Xu et al., 2013). Those features reflect an attempt by macrophages to buffer excess lipids, which is adaptive in the lean state but becomes maladaptive in obese adipose tissue (Boutens and Stienstra, 2016). The lipid-laden macrophages observed in obese adipose tissue are reminiscent of the foamy macrophages present in atherosclerotic plaques. Although foam cell formation and adipose tissue inflammation are known to co-exist in obesity, the exact role of lipid droplet accumulation in adipose tissue macrophages in the development of obesity-induced adipose tissue inflammation and associated metabolic disturbances remains unclear.

HILPDA (hypoxia inducible lipid droplet associated) is a small, lipid-droplet-associated protein expressed in several tissues (Mattijssen et al., 2014). The expression of *Hilpda* is induced by different stimuli, including hypoxia, beta-adrenergic activation, and PPAR transcription factors (Gimm et al., 2010; Mattijssen et al., 2014; Dijk et al., 2017). Gain- and loss-of-function studies have shown that HILPDA promotes lipid deposition in hepatocytes, adipocytes, and macrophages (Gimm et al., 2010; Mattijssen et al., 2014; DiStefano et al., 2015, 2016; Dijk et al., 2017; Maier et al., 2017). The mechanism by which HILPDA promotes lipid storage in cells has not been completely elucidated, but evidence has been presented that HILPDA directly binds and inhibits adipose triglyceride lipase (ATGL) (Zhang et al., 2017; Padmanabha Das et al., 2018), consistent with the ability of HILPDA to inhibit lipolysis (DiStefano et al., 2015; Dijk et al., 2017). Interestingly, endothelial cell marker *Tie2*-Cre-driven deletion of *Hilpda* was found to decrease fatty acid and oxidized low-density lipoprotein (oxLDL)-driven lipid droplet formation in macrophages and reduce lesion formation and progression of atherosclerosis in *Apoe*$^{-/-}$ mice (Maier et al., 2017).

Here, we aimed to determine the exact role of HILPDA in lipid storage in macrophages and to explore the potential causal relationship between lipid droplet accumulation in adipose tissue macrophages and the development of adipose tissue inflammation and insulin resistance during obesity.

RESULTS

Hilpda as Gene of Interest in Obese Adipose Tissue

To identify genes that may be able to modify lipid storage in adipose tissue macrophages, we searched for genes that are induced by lipids and upregulated in adipose tissue macrophages by obesity. To that end, we co-analyzed the transcriptomics data from three experiments: (1) adipose tissue macrophages isolated from obese versus lean mice, (2) mouse peritoneal macrophages treated with the fatty acid oleate, and (3) mouse peritoneal macrophages treated with intralipid, a triglyceride emulsion. Scatterplot analysis identified *Hilpda* as a gene of particular interest (Figure 1A) because it was the only gene that was strongly upregulated in all three experiments. Moreover, *Hilpda* was the most highly induced gene in peritoneal macrophages by oleate. Consistent with a potential role for *Hilpda* in obese-induced adipose tissue inflammation, transcriptome analysis indicated that *Hilpda* expression in adipose tissue is upregulated by high fat feeding in mice, in parallel with macrophage and inflammatory markers, such as *Ccl2* (MCP1), *Cd68*, and *Itgax* (Cd11c) (Figure 1B), as confirmed by qPCR (Figure 1C). Immunohistochemistry of adipose tissue of obese mice indicated that HILPDA co-localized with adipose tissue macrophages in crown-like structures, thus supporting the expression of HILPDA in adipose tissue macrophages (Figure 1D). Together, these data suggest that HILPDA may be implicated in obesity-induced adipose tissue inflammation and foam cell formation.

Hilpda in Macrophages Is Responsive to Lipids

To further investigate the regulation of HILPDA by lipids, we treated RAW264.7 and primary peritoneal macrophages with fatty acids. Confirming the transcriptomics data, oleate markedly upregulated *Hilpda* mRNA in RAW264.7 and peritoneal macrophages (Figure 1E). Similarly, intralipid significantly induced *Hilpda* mRNA in both types of macrophages (Figure 1F). The induction of HILPDA by intralipid in RAW264.7 and peritoneal macrophages was particularly evident at the protein level (Figure 1G). *Hilpda* was originally identified as a hypoxia-inducible gene 2 (*Hig2*) (Denko et al., 2000). Because hypoxic areas are characteristic of obese adipose tissue (Rausch et al., 2008), we tested the effect of a combination of intralipid and a chemical hypoxia mimic. Together, they synergistically increased *Hilpda* mRNA (Figure 1H).

Macrophage-Specific *Hilpda* Deficiency Impairs Lipid Droplet Accumulation

To study the effect of HILPDA on lipid storage in macrophages, we overexpressed HILPDA in RAW264.7 macrophages using an adenoviral vector (Figure 1I). Interestingly, the marked increase in HILPDA protein levels was not accompanied by any changes in lipid droplet accumulation, as visualized by oil red O staining (Figure 1J). These data indicate that overexpression of HILPDA in macrophages has no discernible effect on lipid storage.

We next switched to bone-marrow-derived macrophages (BMDMs) as a robust primary *in vitro* model. Similar to RAW264.7 and peritoneal macrophages, intralipid and chemical hypoxia synergistically upregulated *Hilpda* mRNA in BMDMs (Figure 2A). To be able to study the effects of HILPDA deficiency in macrophages, we generated mice with a myeloid-specific *Hilpda* inactivation (*Hilpda*$^{\Delta M\Phi}$) by crossing *Hilpda*$^{flox/flox}$ with mice expressing Cre-recombinase driven by the LysM promoter. BMDMs obtained from *Hilpda*$^{\Delta M\Phi}$ mice and their *Hilpda*$^{flox/flox}$ littermates were lipid-loaded with a combination of oleate and palmitate for 12 h to induce maximal lipid droplet formation. The Cre-mediated excision in BMDMs led to an approximate 80% reduction in *Hilpda* mRNA (Figure 2B) and a corresponding decrease in HILPDA protein (Figure 2C). Strikingly, staining of neutral lipids by boron-dipyrromethene (BODIPY) in BMDMs showed that lipid droplets were much less visible in fatty acid-loaded *Hilpda*$^{\Delta M\Phi}$ than in *Hilpda*$^{flox/flox}$ macrophages (Figure 2D). Quantitative analysis indicated that the number of lipid droplets per cell and the size of the lipid droplets were significantly lower in *Hilpda*$^{\Delta M\Phi}$ than in *Hilpda*$^{flox/flox}$ macrophages (Figure 2E). This reduction of lipid droplets was confirmed by oil red O staining (Figure 2F). In addition, triglyceride levels were markedly decreased in fatty-acid-loaded *Hilpda*$^{\Delta M\Phi}$ compared with *Hilpda*$^{flox/flox}$ macrophages (Figures 2G and S1). Together, these data show that HILPDA deficiency in macrophages leads to a pronounced decrease in lipid storage.

HILPDA Does Not Regulate Fatty Acid Uptake or Triglyceride Synthesis

We next explored potential mechanisms underlying the decreased lipid storage in HILPDA-deficient macrophages. To determine whether the reduction in lipid storage in HILPDA-deficient macrophages is due to decreased lipid uptake, we measured fatty acid uptake 6 and 35 min after addition of a mixture of oleate and BODIPY-labeled C12 (BODIPY FL). Confocal microscopy showed no difference in fluorescence intensity between *Hilpda*$^{\Delta M\Phi}$ and *Hilpda*$^{flox/flox}$ macrophages at 6

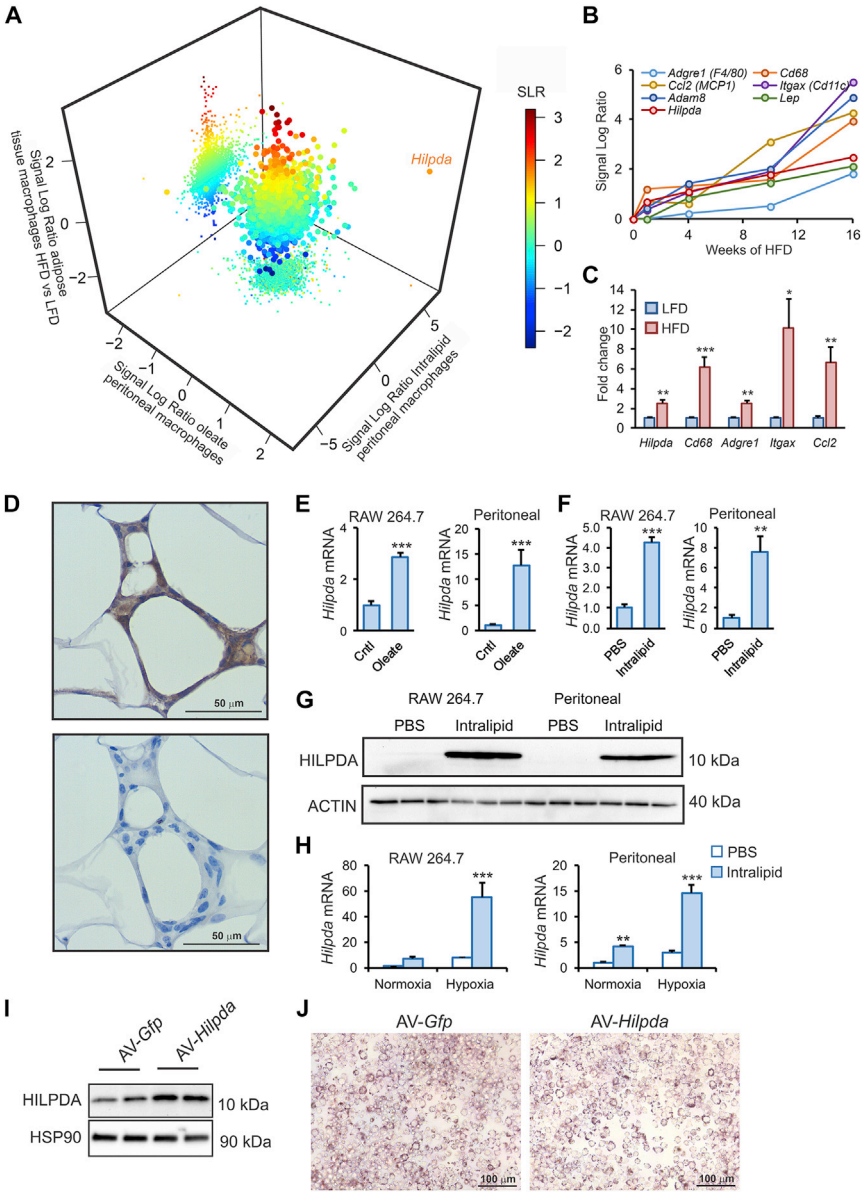

Figure 1. Lipid-Responsive *Hilpda* as Gene of Interest in Obese Adipose Tissue

(A) Transcriptomics co-analysis of ATMs isolated from C57BL/6 mice fed a HFD versus a LFD, C57BL/6 mouse peritoneal macrophages treated with oleate, and C57BL/6 *Angptl4*$^{-/-}$ mouse peritoneal macrophages treated with intralipid.

(B) Signal log-ratio of mRNA patterns of *Hilpda*, inflammatory genes, and macrophage markers in gonadal adipose tissue of C57BL/6 mice fed a HFD for 0, 1, 4, 10, or 16 weeks.

(C) Gene expression of *Hilpda*, *Cd68*, *Adgre1*, *Itgax*, and *Ccl2* in gonadal adipose tissue of C57BL/6 mice fed a HFD for 20 weeks (LFD, n = 8; HFD, n = 10).

(D) Immunohistochemical staining of HILPDA in gonadal adipose tissue from C57BL/6 mice fed a HFD for 20 weeks (representative data for n = 10). Bottom panel is without primary antibody.

(E and F) *Hilpda* mRNA expression in RAW264.7 and C57BL/6 mouse peritoneal macrophages exposed to 250 μM of oleate (E) or 1 mM of intralipid (F) for 6 h versus BSA (control [Cntl]) or PBS.

(G) HILPDA protein levels in RAW264.7 and peritoneal macrophages exposed to 1 mM of intralipid or PBS for 6 h. ACTIN was used as the loading control.

(H) *Hilpda* mRNA expression in RAW264.7 and C57BL/6 mouse peritoneal macrophages exposed to 1 mM of intralipid or PBS in combination with normoxia or a chemical hypoxia mimic induced by 100 μM of 2,2′-bipyridyl for 6 h.

(I) HILPDA protein levels in RAW264.7 macrophages transduced with recombinant adenovirus expressing *Gfp* (AV-*Gfp*) or *Hilpda* (AV-*Hilpda*) at a multiplicity of infection of 500 for 48 h.

(J) Oil red O staining of RAW264.7 macrophages transduced with AV-*Gfp* or AV-*Hilpda*, followed by lipid loading with 667 μM of oleate and 333 μM of palmitate or BSA for 24 h.

Bar graphs are presented as mean ± SEM (*in vivo* studies) or mean ± SD (*in vitro* studies). Statistical testing was performed by Student's t test or by two-way ANOVA followed by Bonferroni's post hoc multiple comparisons test. The effect of treatment was significant in (H). *$p < 0.05$, **$p \leq 0.01$, ***$p \leq 0.001$.

and 35 min (Figure 3A), which was corroborated by quantitative image analysis (Figure 3B), indicating that HILPDA deficiency did not influence fatty acid uptake. Expression of the fatty acid transporter *Cd36* was comparable in *Hilpda*$^{\Delta M\Phi}$ and *Hilpda*$^{flox/flox}$ macrophages (Figure 3C). In addition, the early induction of gene expression by fatty acids was not different between *Hilpda*$^{\Delta M\Phi}$ and *Hilpda*$^{flox/flox}$ macrophages, regardless of whether the fatty acids were provided as free fatty acids (Figure 3D) or intralipids (Figure S2), clearly indicating that HILPDA does not regulate fatty acid uptake. Accordingly, we hypothesized that HILPDA may have two—not necessarily mutually exclusive—functions: (1) activator of fatty acid esterification, and/or (2) inhibitor of triglyceride lipolysis. If HILPDA acts by activating fatty acid esterification in macrophages, suggested before by Maier et al. (2017), it would be expected that HILPDA deficiency would lead to accumulation of intermediates in the triglyceride synthesis pathway. To explore that possibility, we performed shotgun lipidomics on *Hilpda*$^{\Delta M\Phi}$ and *Hilpda*$^{flox/flox}$ BMDMs loaded with oleate:palmitate for 24 h. Partial least-squares discriminant analysis clearly separated the two genotypes (Figure 3E), indicating that the lipidomics profiles of *Hilpda*$^{\Delta M\Phi}$ and *Hilpda*$^{flox/flox}$ macrophages are very distinct. Volcano plot analysis indicated that, although a number of lipids were increased in *Hilpda*$^{\Delta M\Phi}$ macrophages, most lipids were reduced (Figure 3F). Indeed, levels of phosphatidic acids, diacylglycerols, and triglycerides were significantly decreased in *Hilpda*$^{\Delta M\Phi}$ versus *Hilpda*$^{flox/flox}$ macrophages (Figure 3G) as were cholesteryl esters, whereas lysophosphatidic acids were hardly detectable. The decrease in triglycerides and diacylglycerols was accounted for by the major subspecies within each lipid

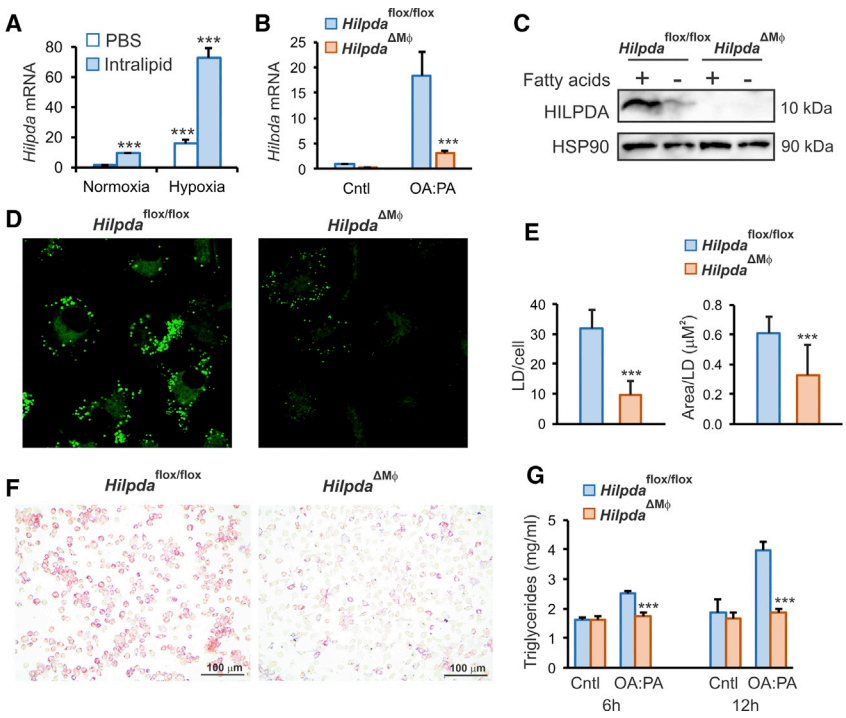

Figure 2. Myeloid-Specific HILPDA Deficiency Decreases Lipid Droplet Accumulation

(A) *Hilpda* mRNA expression in C57BL/6 BMDMs exposed to 1 mM of intralipid or PBS, combined with normoxia or chemical hypoxia induced by 100 μM of 2,2′-bipyridyl for 6 h.

(B and C) Gene expression of *Hilpda* (B) and protein levels of HILPDA (C) in *Hilpda*$^{flox/flox}$ and *Hilpda*$^{\Delta M\Phi}$ BMDMs lipid loaded with 400 μM of oleate and 200 μM of palmitate (OA:PA, Fatty acids) or BSA (Cntl) for 12 h (n = 3). HSP90 was used as loading control.

(D–F) BODIPY (D and E) and oil red O (F) staining in *Hilpda*$^{flox/flox}$ and *Hilpda*$^{\Delta M\Phi}$ BMDMs lipid loaded with oleate:palmitate or BSA (Cntl) for 24 h. Data are shown from or are representative of at least three independent experiments.

(G) Triglyceride measurement in BMDMs from *Hilpda*$^{flox/flox}$ and *Hilpda*$^{\Delta M\Phi}$ lipid loaded with oleate:palmitate or BSA (Cntl) for 6 or 12 h. See also Figure S1.

Bar graphs are presented as mean ± SD. Statistical testing was performed by Student's t test or by two-way ANOVA followed by Bonferroni's post hoc multiple comparisons test. The effect of treatment was significant in (A), (B) and (G). *$p < 0.05$, ***$p \leq 0.001$. LD, lipid droplet; OA:PA, oleate:palmitate.

class (Figure 3H). These data suggest that HILPDA probably does not regulate the fatty acid esterification pathway in macrophages.

HILPDA Regulates Lipid Droplet Mobilization through ATGL Inhibition

To further investigate the molecular basis for the decreased lipid storage in HILPDA-deficient macrophages, we determined the trafficking of lipids after loading with a mixture of oleate and BODIPY FL for either 5 or 24 h. Strikingly, after lipid loading *Hilpda*$^{flox/flox}$ macrophages for 5 h, the BODIPY FL had largely accumulated in lipid droplets, whereas in *Hilpda*$^{\Delta M\Phi}$ macrophages, the BODIPY FL was mainly distributed throughout the endoplasmic reticulum (ER) and showed only minor presence in lipid droplet-like structures (Figure 4A). After lipid loading for 24 h, the size and number of lipid droplets had further increased in *Hilpda*$^{flox/flox}$ macrophages, whereas in *Hilpda*$^{\Delta M\Phi}$ macrophages, the lipid-droplet-like structures that had initially formed at 5 h were no longer visible (Figure 4A). These data indicate that *Hilpda*$^{\Delta M\Phi}$ BMDMs, although able to take up similar amounts of fatty acids as *Hilpda*$^{flox/flox}$ BMDMs, are unable to retain them in lipid droplets.

Using various biochemical and cellular assays, we and others previously found that HILPDA is able to inhibit ATGL, the rate-limiting enzyme for lipolysis (Zhang et al., 2017; Padmanabha Das et al., 2018). However, it is unclear whether HILPDA is a physiological regulator of ATGL in macrophages. To investigate whether the decrease in lipid droplet and triglyceride accumulation in *Hilpda*$^{\Delta M\Phi}$ macrophages is due to enhanced ATGL-mediated lipolysis, we loaded *Hilpda*$^{\Delta M\Phi}$ and *Hilpda*$^{flox/flox}$ BMDMs with oleate:palmitate in the presence of Atglistatin, a small-molecule inhibitor of ATGL (Mayer et al., 2013). Strikingly, inhibiting ATGL markedly increased lipid droplets in *Hilpda*$^{\Delta M\Phi}$ BMDMs (Figure 4B), almost completely rescuing the *Hilpda*$^{\Delta M\Phi}$ phenotype. Quantitative analysis showed that the lipid droplet surface area was not significantly affected by Atglistatin in *Hilpda*$^{flox/flox}$ BMDMs and markedly increased by Atglistatin in *Hilpda*$^{\Delta M\Phi}$ BMDMs (Figure S3A). Similarly, the defective retention of BODIPY FL in lipid droplets in *Hilpda*$^{\Delta M\Phi}$ macrophages was almost completely abolished by Atglistatin (Figures 4C and S3B). These studies indicate that the decrease in lipid droplet and triglyceride accumulation in *Hilpda*$^{\Delta M\Phi}$ macrophages is caused by accelerated lipid droplet breakdown via enhanced ATGL-mediated lipolysis. Our data thus suggest that HILPDA functions as a potent endogenous inhibitor of ATGL in macrophages.

To determine whether HILPDA may influence the abundance of ATGL and other lipid droplet-associated proteins in macrophages, we performed western blot on *Hilpda*$^{\Delta M\Phi}$ and *Hilpda*$^{flox/flox}$ BMDMs loaded with oleate:palmitate for 24 h. As expected, lipid loading increased HILPDA levels as well as PLIN3 levels (Figure 4D). Remarkably, ATGL levels were markedly higher in *Hilpda*$^{\Delta M\Phi}$ than in *Hilpda*$^{flox/flox}$ BMDMs, suggesting that HILPDA not only inhibits ATGL but also decreases ATGL protein levels. G0S2 protein levels, despite being difficult to detect, were also higher in *Hilpda*$^{\Delta M\Phi}$ than in *Hilpda*$^{flox/flox}$ BMDMs.

HILPDA Deficiency Promotes Respiration

If lipolysis is enhanced, the free fatty acid levels in the cell may rise, thereby stimulating fatty-acid-dependent gene regulation. Consistent with this notion, the expression of fatty-acid-inducible *Gdf15*, *Cpt1a*, and *Il7r* was significantly higher in lipid-loaded *Hilpda*$^{\Delta M\Phi}$ than in *Hilpda*$^{flox/flox}$ BMDMs (Figure 5A). To analyze that further, we performed transcriptomics on *Hilpda*$^{\Delta M\Phi}$ and

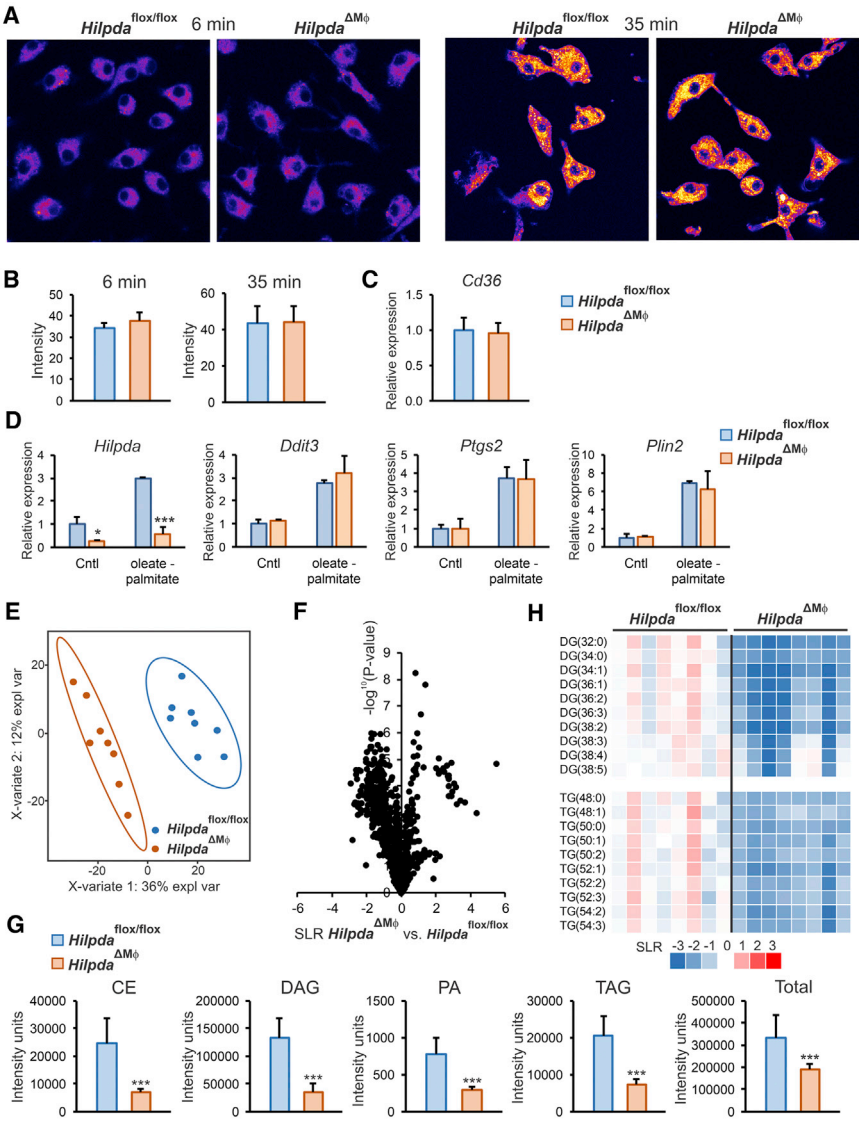

Figure 3. HILPDA Does Not Regulate Fatty Acid Uptake or Triglyceride Synthesis

(A) Confocal microscopy of *Hilpda*$^{flox/flox}$ and *Hilpda*$^{\Delta M\Phi}$ BMDMs incubated with BODIPY FL for 6 or 35 min.

(B) Fluorescence quantification reflecting fatty acid uptake.

(C) *Cd36* mRNA in *Hilpda*$^{flox/flox}$ and *Hilpda*$^{\Delta M\Phi}$ BMDMs.

(D) Gene expression of *Hilpda*, *Ddit3*, *Ptgs2*, and *Plin2* in BMDMs from *Hilpda*$^{flox/flox}$ and *Hilpda*$^{\Delta M\Phi}$ lipid loaded with oleate:palmitate or BSA (Cntl) for 6 h (n = 3). See also Figure S2.

(E–H) Partial least-square discriminant analysis (E); volcano plot analysis (F); differences in abundancy of cholesteryl esters (CE), diacylglycerol (DAG), phosphatidic acid (PA), triacylglycerol (TAG), and total lipid species (G); and heatmap of most-abundant DAG and TAG species (H) based on shotgun lipidomics on *Hilpda*$^{flox/flox}$ and *Hilpda*$^{\Delta M\Phi}$ BMDMs loaded with oleate:palmitate for 24 h.

Bar graphs are presented as mean ± SD. Statistical testing was performed by Student's t test or by two-way ANOVA followed by Bonferroni's post hoc multiple comparisons test. The effect of treatment was significant in (C). *p < 0.05, ***p ≤ 0.001. SLR, signal log ratio.

Hilpda$^{flox/flox}$ BMDMs loaded with oleate:palmitate for 24 h and co-analyzed the data together with a transcriptomics dataset of Robblee et al. (2016) on wild-type BMDMs loaded with stearate for 20 h, as well as with the transcriptomics dataset of adipose tissue macrophages from obese and lean mice. In line with enhanced fatty-acid-dependent gene regulation in *Hilpda*-deficient macrophages, genes that were highly upregulated after stearate in wild-type BMDMs, such as *Gdf15*, *Il7r*, and *Ddit3*, were also higher in fatty-acid-loaded *Hilpda*$^{\Delta M\Phi}$ than *Hilpda*$^{flox/flox}$ BMDMs (Figure 5B). In addition, pro-inflammatory genes, such as *Ccl2* and *Il1b*, were downregulated by stearate in wild-type BMDMs and were also lower in fatty-acid-loaded *Hilpda*$^{\Delta M\Phi}$ compared with *Hilpda*$^{flox/flox}$ BMDMs. Interestingly, genes induced by obesity in adipose tissue macrophages, such as *Lpl*, *Lipa*, and *Itgax*, were only weakly regulated by stearate and by HILPDA deficiency, suggesting distinct regulatory mechanisms (Figure 5B).

Of the 6,600 genes that passed the expression threshold, only 49 were induced more than 2-fold in fatty-acid-loaded *Hilpda*$^{\Delta M\Phi}$ compared with *Hilpda*$^{flox/flox}$ BMDMs. The limited effect of impaired triglyceride retention in *Hilpda*$^{\Delta M\Phi}$ BMDMs suggests that the excess fatty acids may be disposed of, for instance, by enhanced oxidation. To explore that option, cellular respiration was determined in fatty-acid-loaded *Hilpda*$^{\Delta M\Phi}$ and *Hilpda*$^{flox/flox}$ BMDMs. As a marker for oxidative phosphorylation, oxygen consumption of fatty-acid-loaded *Hilpda*$^{\Delta M\Phi}$ and *Hilpda*$^{flox/flox}$ BMDMs was measured by extracellular flux analysis during a mitochondrial stress test (Figure 5C). After 6 h of oleate:palmitate loading, basal and maximal respiration were slightly lower in *Hilpda*$^{\Delta M\Phi}$ than in *Hilpda*$^{flox/flox}$ BMDMs (Figure 5D). Remarkably, however, after 24 h of fatty acid loading, basal and maximal respiration were significantly higher in *Hilpda*$^{\Delta M\Phi}$ compared with *Hilpda*$^{flox/flox}$ BMDMs (Figure 5D), indicating an increased maximal oxidative capacity. These data suggest that the enhanced lipolysis in *Hilpda*$^{\Delta M\Phi}$ BMDMs is accompanied by increased fatty acid oxidation through oxidative phosphorylation.

Next, we tested whether HILPDA might influence lipid droplet accumulation in macrophages in adipose tissue. To mimic the adipose environment *in vitro*, BMDMs were treated with conditioned medium of adipose tissue explants. Adipose-conditioned medium markedly increased *Hilpda* expression, along with that of several other lipid-sensitive genes, such as *Plin2*, *Cd36*, and

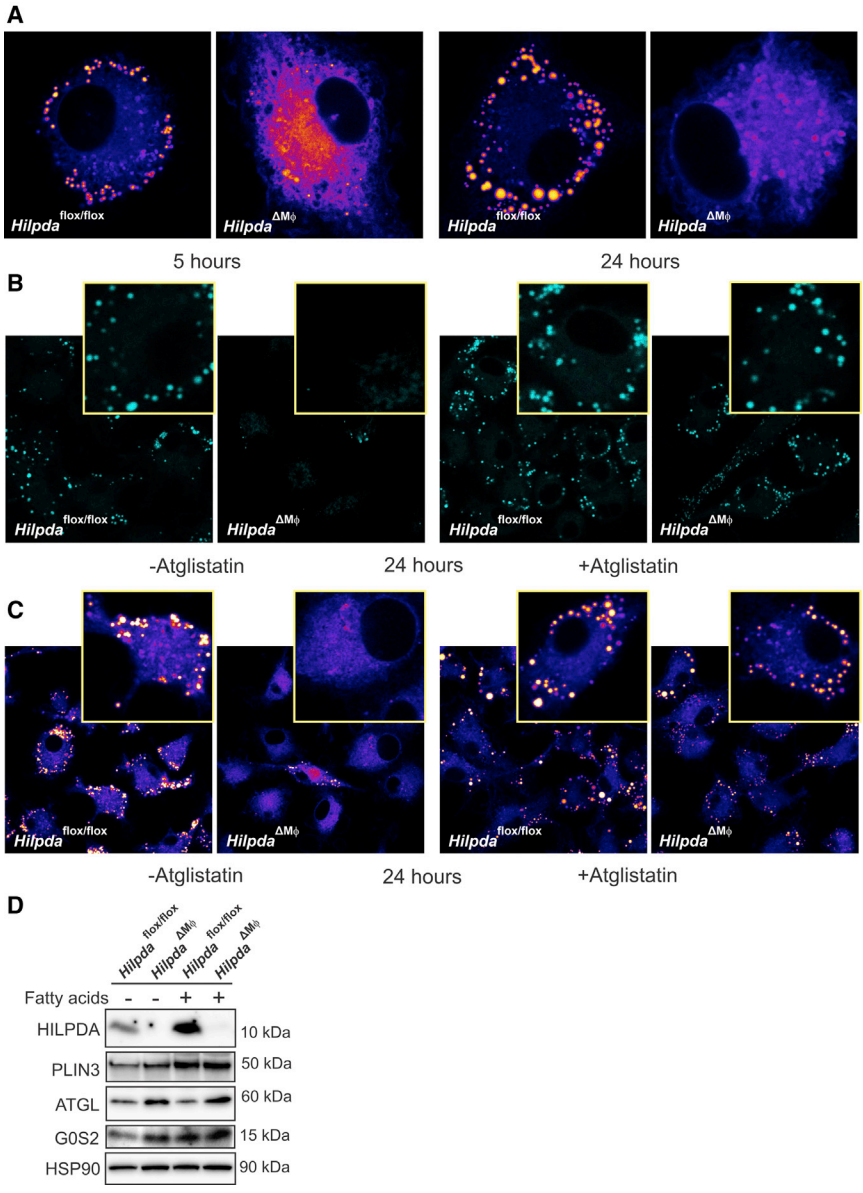

Figure 4. HILPDA Regulates Lipid Droplet Mobilization through ATGL Inhibition

(A) Fatty acid trafficking in *Hilpda*$^{flox/flox}$ and *Hilpda*$^{\Delta M\Phi}$ BMDMs lipid-loaded with oleate and BODIPY FL for 5 or 24 h.

(B) BODIPY staining in *Hilpda*$^{flox/flox}$ and *Hilpda*$^{\Delta M\Phi}$ BMDMs lipid-loaded with oleate:palmitate for 24 h and treated with 20 μM of Atglistatin or vehicle.

(C) Fatty acid trafficking in *Hilpda*$^{flox/flox}$ and *Hilpda*$^{\Delta M\Phi}$ BMDMs lipid-loaded with oleate and BODIPY FL for 24 h and treated with 20 μM of Atglistatin or vehicle.

(D) Protein expression of selected lipid droplet-associated proteins in *Hilpda*$^{flox/flox}$ and *Hilpda*$^{\Delta M\Phi}$ BMDMs lipid-loaded with oleate:palmitate or BSA for 12 h.

LD, lipid droplet.

See also Figure S3.

Angptl4 (Figure 5E). Consistent with our previous studies with fatty-acid-loaded macrophages, *Hilpda*$^{\Delta M\Phi}$ BMDMs incubated with adipose-conditioned medium showed substantially reduced BODIPY staining compared with *Hilpda*$^{flox/flox}$ BMDMs (Figure 5F). These data suggest that HILPDA may also influence lipid droplet accumulation in macrophages in adipose tissue.

Myeloid-Specific Deficiency of HILPDA Decreases Lipid Droplets in Adipose Tissue Macrophages (ATMs) without Altering Adipose Tissue Inflammation

To enable studying the effect of HILPDA deficiency in macrophages *in vivo*, we used *Hilpda*$^{\Delta M\Phi}$ mice and their *Hilpda*$^{flox/flox}$ littermates. As expected, myeloid-specific inactivation of *Hilpda* significantly decreased *Hilpda* expression in the stromal vascular fraction of the adipose tissue but not in the adipocyte fraction (Figure 6A). To test the functional consequences of macrophage HILPDA deficiency in the context of obesity-induced adipose tissue inflammation and foam cell formation, *Hilpda*$^{\Delta M\Phi}$ mice and their *Hilpda*$^{flox/flox}$ littermates were rendered obese and insulin resistant by high fat feeding for 20 weeks, using a low-fat diet as control. Bodyweight gain (Figure 6B), feed intake (Figure 6C), and liver and adipose tissue weights (Figure 6D) were not different between *Hilpda*$^{\Delta M\Phi}$ and *Hilpda*$^{flox/flox}$ littermates. Consistent with the data shown in Figure 1C, high-fat feeding increased *Hilpda* mRNA in adipose tissue. Interestingly, the relative increase in *Hilpda* mRNA was considerably lower in *Hilpda*$^{\Delta M\Phi}$ than it was in *Hilpda*$^{flox/flox}$ adipose tissue (Figure 6E), suggesting that the increase in *Hilpda* expression by high-fat feeding is mainly driven by its expression in macrophages. Immunoblot for HILPDA confirmed that notion by showing markedly reduced HILPDA protein levels in *Hilpda*$^{\Delta M\Phi}$ versus *Hilpda*$^{flox/flox}$ adipose tissue (Figure 6F).

Based on the studies in BMDMs, we hypothesized that lipid accumulation would be reduced in adipose tissue macrophages from *Hilpda*$^{\Delta M\Phi}$ mice compared with *Hilpda*$^{flox/flox}$ mice. Indeed, oil red O staining showed significantly lower lipid droplet content in adipose tissue macrophages isolated from high-fat diet (HFD)-fed *Hilpda*$^{\Delta M\Phi}$ mice compared with HFD-fed *Hilpda*$^{flox/flox}$ mice (Figures 7A and 7B). Interestingly, however, the decrease in lipid droplets was not associated with any change in the secretion of the classical inflammatory cytokines interleukin-6 (IL-6) and tumor necrosis factor alpha (TNF-α) (Figure 7C). These data indicate that HILPDA deficiency reduces lipid accumulation in adipose tissue macrophages but does not have any effect on their *ex vivo* inflammatory properties.

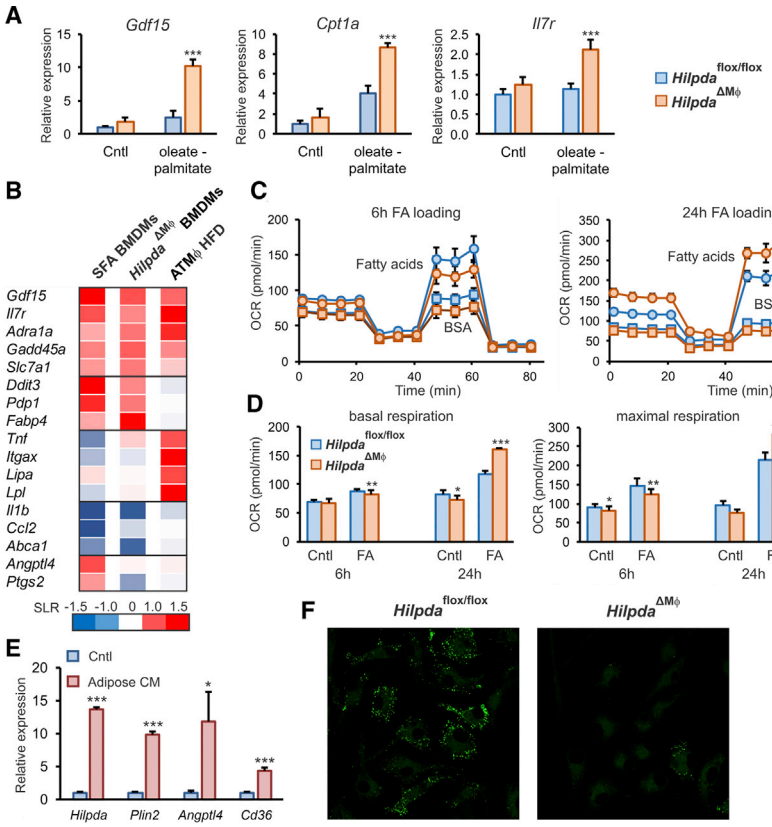

Figure 5. Loss of ATGL Inhibition by HILPDA Deficiency Does Not Affect Lipid-Induced Inflammation but Increases Oxidative Respiration

(A) Gene expression of *Gdf15*, *Cpt1a*, *Il7r*, and *Fabp4* in *Hilpda*$^{flox/flox}$ and *Hilpda*$^{\Delta M\Phi}$ BMDMs lipid-loaded with oleate:palmitate or BSA (Cntl) for 12 h (n = 3).

(B) Microarray-based gene expression of relevant genes in wild-type (WT) C57BL/6 mouse BMDMs loaded with stearate (250 μM) for 20 h, *Hilpda*$^{\Delta M\Phi}$ BMDMs loaded with oleate:palmitate for 24 h, and adipose tissue macrophages isolated from mice fed a HFD versus a LFD.

(C and D) Oxygen consumption rate of *Hilpda*$^{flox/flox}$ and *Hilpda*$^{\Delta M\Phi}$ BMDMs lipid-loaded with oleate:palmitate or BSA (Cntl) for 6 or 24 h (C) and corresponding basal and maximal respiration levels (D). Data are representative of three independent experiments.

(E and F) Gene expression levels of *Hilpda*, *Plin2*, *Angptl4*, and *Cd36* in C57BL/6 mouse BMDMs loaded with adipose-conditioned medium (CM) or Cntl for 6 h (E) and BODIPY staining after loading with CM for 24 h (F) (n = 3).

Bar graphs are presented as mean ± SD. Statistical testing was performed by Student's t test or by two-way ANOVA followed by Bonferroni's post hoc multiple comparisons test. The effect of treatment was significant in (A) and (D). *p < 0.05, **p ≤ 0.01, ***p ≤ 0.001. FA, fatty acid loading with oleate:palmitate; SLR, signal log ratio.

To investigate the potential effect of macrophage HILPDA on adipose tissue inflammation *in vivo*, we performed flow cytometry analysis of the stromal vascular fraction isolated from the adipose tissue of the various groups of mice. The results showed an increased percentage of populations of $CD45^+$, $CD11b^+CD206^+$, and $CD11b^+CD11c^+$ cells by high-fat feeding, but no clear differences in the percentages of those populations between *Hilpda*$^{\Delta M\Phi}$ and *Hilpda*$^{flox/flox}$ mice (Figure 7D). To further examine the influence of macrophage HILPDA deficiency on inflammation in adipose tissue, we determined the expression of selected genes. Interestingly, mRNA levels of both inflammatory macrophage marker *Itgax* (Cd11c) and general macrophage marker *Cd68* were significantly lower in adipose tissue of *Hilpda*$^{\Delta M\Phi}$ mice versus *Hilpda*$^{flox/flox}$ mice fed a HFD (Figure 7E), whereas the general macrophage marker *Adgre1* (F4/80) showed a trend toward a decreased expression (Figure S4). Despite being induced by high-fat feeding, adipose expression of other pro- or anti-inflammatory genes, such as *Gdf15*, *Il10*, *Arg1*, *Ccl2*, and *Il1ra*, was not significantly different between *Hilpda*$^{\Delta M\Phi}$ and *Hilpda*$^{flox/flox}$ mice (Figure S4). Expression of *Adipoq* and *Leptin* also was not different between *Hilpda*$^{\Delta M\Phi}$ and *Hilpda*$^{flox/flox}$ mice (Figure S4).

To further investigate the inflammatory status of adipose tissue, the density of crown-like structures was determined in adipose tissue of *Hilpda*$^{\Delta M\Phi}$ and *Hilpda*$^{flox/flox}$ mice fed a HFD. A trend toward lower density was found in the *Hilpda*$^{\Delta M\Phi}$ mice (Figure 7F), which, however, did not reach statistical significance (Figure 7G). Additionally, we measured the *ex vivo* release of cytokines from adipose tissue explants. Although high-fat feeding stimulated the release of IL-10 and IL-6, no significant difference in IL-10 and IL-6 release was observed between adipose tissue explants from *Hilpda*$^{\Delta M\Phi}$ and *Hilpda*$^{flox/flox}$ mice (Figure 7H).

Finally, to determine whether macrophage HILPDA deficiency has any influence on obesity-induced metabolic derailments, we measured plasma metabolic parameters and assessed glucose tolerance in *Hilpda*$^{\Delta M\Phi}$ and *Hilpda*$^{flox/flox}$ mice fed the low- and high-fat diets. High-fat feeding significantly increased plasma levels of cholesterol, triglycerides, glucose, non-esterified fatty acids, leptin, and insulin (Figure S5). However, no differences in those parameters were observed between *Hilpda*$^{\Delta M\Phi}$ and *Hilpda*$^{flox/flox}$ mice, either on a low- or high-fat diet (Figure S5). Similarly, although high-fat feeding caused a marked decrease in glucose tolerance, no differences were observed between *Hilpda*$^{\Delta M\Phi}$ and *Hilpda*$^{flox/flox}$ mice (Figure 7I).

Collectively, our data indicate that myeloid-specific HILPDA deficiency reduces lipid droplet accumulation in adipose tissue macrophages but does not influence the inflammatory status of adipose tissue and does not have any effect on obesity-induced metabolic complications.

DISCUSSION

Here, we show that HILPDA deficiency in macrophages disrupts stable lipid droplet formation after lipid loading. The reduction in

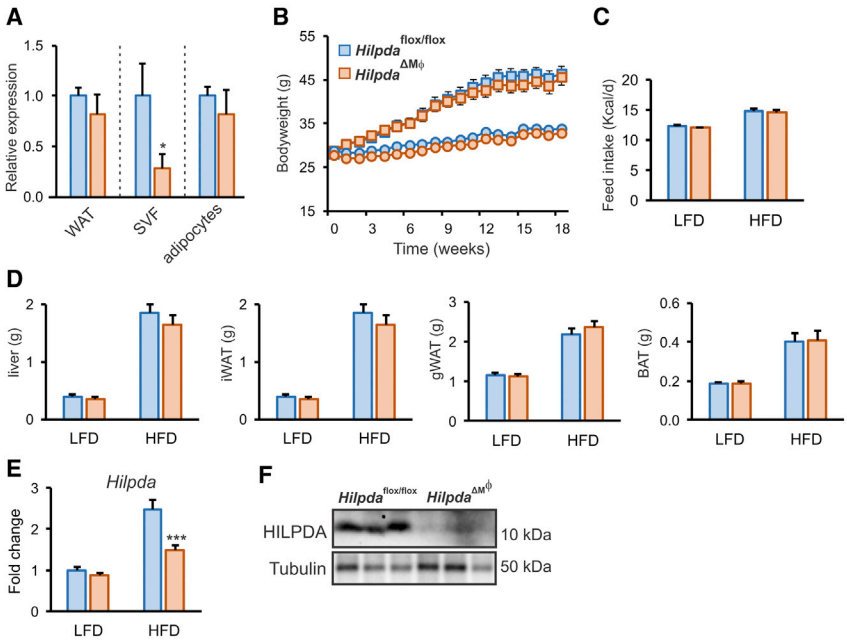

Figure 6. *Hilpda* Deficiency in Myeloid Cells Results in a Decrease in HILPDA in Gonadal White Adipose Tissue (gWAT) after High-Fat Feeding, without Influencing Body and Organ Weight

(A) Relative gene expression of *Hilpda* in whole gWAT, stromal vascular fraction, and adipocyte fraction of *Hilpda*$^{flox/flox}$ and *Hilpda*$^{\Delta M\Phi}$ mice (n = 3–7).

(B–F) Body weight (B), feed intake (C), and weight of liver, inguinal white adipose tissue (iWAT), gWAT, and BAT (D) in *Hilpda*$^{flox/flox}$ and *Hilpda*$^{\Delta M\Phi}$ mice fed a LFD or a HFD for 20 weeks. *Hilpda* gene expression in gWAT (E) and HILPDA protein expression in gWAT (F).

Bar graphs are presented as mean ± SEM, (n = 10–12 mice per group). Statistical testing was performed by Student's t test or by two-way ANOVA followed by Bonferroni's post hoc multiple comparisons test. The effect of diet was significant in (C), (D), and (E). *p < 0.05, ***p ≤ 0.001. BAT, brown adipose tissue; gWAT, gonadal adipose tissue; iWAT, inguinal adipose tissue; SVF, stromal vascular fraction.

lipid droplets is caused by impaired retention of lipids because of elevated ATGL-mediated lipolysis, which, in turn, is associated with increased oxidative metabolism (Figure S6). Overall, our data demonstrate that HILPDA is an endogenous and physiological inhibitor of ATGL in macrophages. Strikingly, despite reducing lipid storage in adipose tissue macrophages, HILPDA deficiency in macrophages does not alter the inflammatory status of adipose tissue in diet-induced obesity, arguing against the notion that lipid droplet accumulation in adipose tissue macrophages promotes adipose tissue inflammation and associated metabolic complications, such as insulin resistance.

During obesity, macrophages infiltrate the adipose tissue and take up adipocyte-released lipids. The resulting lipid-laden macrophages are found in crown-like structures in murine and human obesity (Lumeng et al., 2008; Prieur et al., 2011; Shapiro et al., 2013). These macrophages form a distinct subpopulation with a characteristic activation that is likely triggered by the adipocyte-released lipids (Kratz et al., 2014; Coats et al., 2017; Hill et al., 2018). Because lipid droplet formation often serves as a cytoprotective mechanism to prevent lipotoxicity by lipid intermediates or free fatty acids (Saraswathi and Hasty, 2009), it could be hypothesized that the enhanced lipid droplet breakdown in HILPDA-deficient macrophages may result in elevated inflammation. However, HILPDA deficiency not only reduced intracellular triglyceride levels but also the levels of potentially lipotoxic intermediates, such as diacylglycerols, likely via enhanced fatty acid oxidation, which may be predicted to lead to reduced inflammation (Namgaladze and Brüne, 2016). Intriguingly, however, no clear effect of HILPDA deficiency was observed on cytokine release by adipose tissue macrophages, on the percentage of different macrophage populations in adipose tissue, on inflammatory gene expression in adipose tissue, and on cytokine release by adipose tissue explants. In addition, genes typically elevated in adipose tissue macrophages of obese mice, such as *Lipa*, *Lpl*, and *Itgax*, were not induced by fatty acid loading or altered by HILPDA deficiency. The data argue against the notion that excessive lipid droplet accumulation in adipose tissue macrophages is the major driver of adipose tissue inflammation and of the composition of macrophage populations in obese adipose tissue. Rather, the unique profile of adipose tissue macrophages may be determined by other factors active in the obese adipose tissue environment, the identity of which requires further study.

As indicated above, HILPDA-deficient macrophages exhibited a marked decrease in intracellular levels of all the major lipid species, including triglycerides, diacylglycerols, phosphatidic acids, and cholesteryl esters, likely because of enhanced fatty acid oxidation. Previously, a strong link was made between ATGL activity and fatty acid oxidation in liver and heart. It was found that ATGL-mediated lipolysis activates a transcriptional network involving PGC-1α/PPAR-α that controls fatty acid oxidation and mitochondrial biogenesis (Reid et al., 2008; Sapiro et al., 2009; Haemmerle et al., 2011; Ong et al., 2011). Accordingly, it is likely that the loss of ATGL inhibition is directly responsible for the enhanced oxidative capacity, reducing the total intracellular lipid levels. In general, increased lipolysis and increased oxidative respiration are two traits essential for macrophage polarization toward alternative, M2-like phenotypes, which may be protective in the context of adipose tissue inflammation (Huang et al., 2014; Van den Bossche et al., 2016; Jung et al., 2018). In our experiments, increased oxidative respiration seemed a mere consequence following overactive ATGL-mediated lipolysis and did not contribute to any anti-inflammatory effects. Although increased oxidation of fatty acids is often proposed as an alternative cytoprotective pathway in lipid-laden macrophages, the interplay between fatty acid oxidation, concomitant reactive oxygen

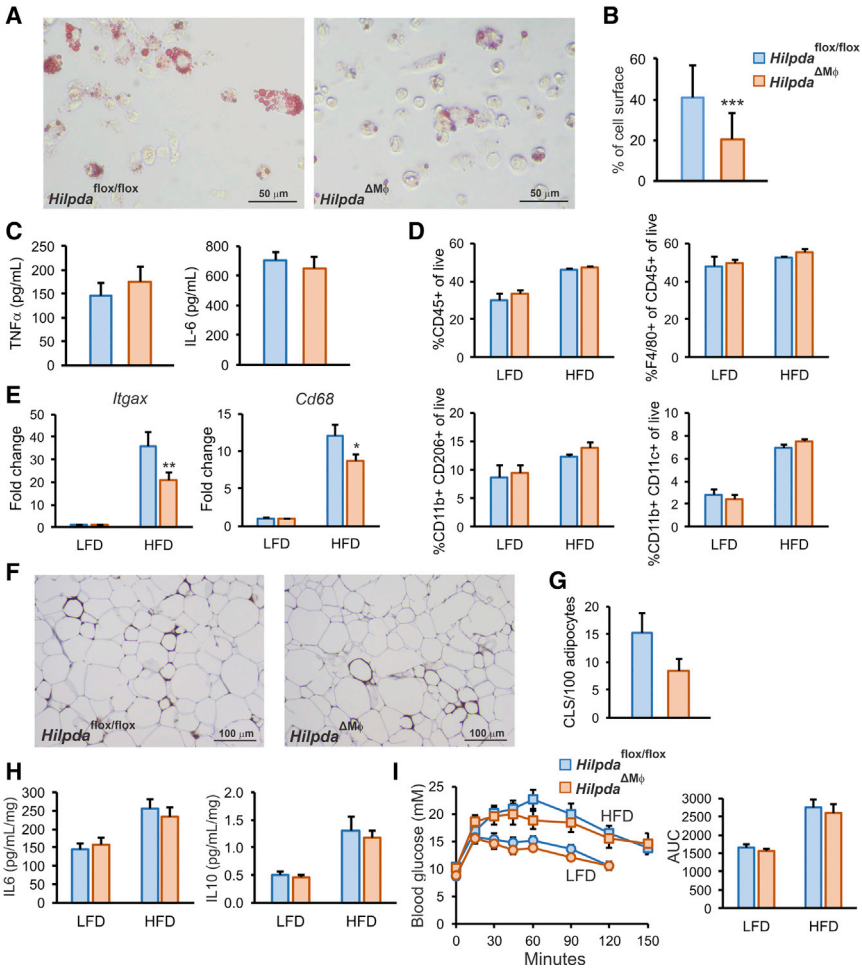

Figure 7. Myeloid-Specific Deficiency of *Hilpda* Decreases Lipid Droplets in ATMs without Altering Adipose Tissue Inflammation or Glucose Tolerance

(A) Oil red O staining of adipose tissue macrophages isolated from *Hilpda*$^{flox/flox}$ and *Hilpda*$^{\Delta M\Phi}$ mice fed a HFD for 20 weeks.

(B) Quantification of Oil red O staining. Data are mean ± SD.

(C) Corrected TNF-α and IL-6 secretion of adipose tissue macrophages from *Hilpda*$^{flox/flox}$ and *Hilpda*$^{\Delta M\Phi}$ mice fed a HFD for 20 weeks (n = 10–12 per group, pooled per 3–4).

(D) Flow-cytometry-based percentages of CD45$^+$, CD45$^+$F4/80$^+$, CD11b$^+$CD206$^+$, and CD11b$^+$ CD11c$^+$ populations in the SVF of gWAT from *Hilpda*$^{flox/flox}$ and *Hilpda*$^{\Delta M\Phi}$ mice (n = 10–12, pooled per 3–4).

(E) Gene expression of *Itgax*, *Adgre1*, *Cd68*, *Ccl2*, *Il10*, and *Il1ra*; see also Figure S4.

(F–H) Density of CLSs in gWAT coupes stained for F4/80 from *Hilpda*$^{flox/flox}$ (F) and *Hilpda*$^{\Delta M\Phi}$ (G) mice (only for HFD) and secretion of IL-6 and IL-10 (H) in gWAT explants (n = 10–12 per group).

(I) Glucose tolerance test after 18 weeks of LFD or HFD feeding; see also Figure S5.

Bar graphs are presented as mean ± SEM, (n = 10–12 mice per group). Statistical testing was performed by Student's t test or by two-way ANOVA followed by Bonferroni's post hoc multiple comparisons test. The effect of diet was significant in (D), (E), (H), and the AUCs of (I). *p < 0.05, **p ≤ 0.01, ***p ≤ 0.001. AUC, area under the curve; CLS, crown-like structure; SVF, stromal vascular fraction; .

species (ROS) formation, and ER stress complicates this mechanism (Namgaladze and Brüne, 2016).

Apart from fatty acid oxidation, ATGL has also been linked to the autophagic degradation of lipid droplets, termed lipophagy (Sathyanarayan et al., 2017). It was suggested that ATGL acts as a signaling node to promote lipophagy, which then controls bulk lipid-droplet breakdown. Whether HILPDA, via ATGL, connects to lipophagy requires further study.

In contrast to the cytoprotective effect of normal lipid droplet formation, the adverse effects of excessive triglyceride storage becomes apparent in ATGL$^{-/-}$ macrophages, underlining the importance of functional ATGL in macrophages (Chandak et al., 2010; Aflaki et al., 2011a, 2011b, 2012). Indeed, the elevated triglyceride accumulation in ATGL$^{-/-}$ macrophages is accompanied by mitochondrial dysfunction and apoptosis, ER stress, reduced macrophage migration, and decreased phagocytosis ability (Chandak et al., 2010; Aflaki et al., 2011a, 2011b, 2012), suggesting that proper macrophage function is dependent on the liberation of free fatty acids from intracellular triglyceride stores. The ATGL-mediated release of fatty acids is also necessary for the production of lipid mediators, at least in neutrophils (Schlager et al., 2015). Similar to ATGL$^{-/-}$ macrophages, macrophages deficient in the ATGL activator CGI-58 (also known as ABHD5) also have elevated lipid storage and decreased phagocytic capacity but show no signs of mitochondrial apoptosis and ER stress, suggesting that triglyceride accumulation per se does not drive mitochondrial dysfunction (Goeritzer et al., 2014). Our data show that HILPDA deficiency, despite leading to markedly reduced lipid storage, raises markers of ER stress, suggesting that triglyceride storage protects against lipid-induced ER stress. Presumably, the mechanism leading to ER stress is different in HILPDA-deficient macrophages as compared with ATGL/CGI-58-deficient macrophages.

HILPDA was initially identified in a screen for hypoxia-inducible genes in human cervical cancer cells and was later found to be associated with lipid droplets (Denko et al., 2000; Gimm et al., 2010). We identified *Hilpda* as a novel PPARα target gene in liver (Mattijssen et al., 2014). In addition, *Hilpda* is well expressed in adipocytes (DiStefano et al., 2016; Dijk et al., 2017). Several studies have shown that overexpression of *Hilpda* increases intracellular lipid storage in cells (Gimm et al., 2010; Mattijssen et al., 2014; Dijk et al., 2017). In the present study, *Hilpda* emerged from a screen for genes elevated by obesity in adipose tissue macrophages and upregulated in macrophages by fatty acids. Induction of HILPDA by fatty acids and subsequent inhibition of triglyceride hydrolysis is likely part of a lipid-buffering effort of the cell to effectively store excess energy and neutralize the potentially reactive free fatty acids (Figure S6).

The observation that the decrease in lipid storage in HILPDA-deficient macrophages can be almost completely abolished by inhibition of ATGL indicates that HILPDA is an endogenous inhibitor of ATGL in macrophages, which is in line with previous data showing direct inhibition of ATGL by HILPDA (Zhang et al., 2017; Padmanabha Das et al., 2018). Intriguingly, HILPDA reduced ATGL protein levels in BMDMs, which supports our previous finding that HILPDA reduces ATGL protein levels in 3T3-L1 adipocytes (Dijk et al., 2017). It can be hypothesized that binding of HILPDA to ATGL might destabilize it, leading to enhanced ATGL degradation. This option should be investigated in future experiments. Of note, our observation that forced upregulation of HILPDA levels in macrophages does not noticeably increase lipid-droplet accumulation suggests that inhibition of ATGL is nearly maxed out in lipid-loaded macrophages.

The inhibition of ATGL by HILPDA is analogous to the inhibition by G_0/G_1 switch gene 2 (G0S2), with which HILPDA shares extensive sequence homology (Yang et al., 2010; Zhang et al., 2017; Padmanabha Das et al., 2018). However, the inhibitory potency of HILPDA was low compared with G0S2, which raised questions on the physiological relevance of HILPDA as an ATGL inhibitor. Our studies demonstrate that HILPDA is a potent endogenous inhibitor of ATGL-mediated lipolysis in macrophages. A number of questions emerge from this work. First, why does HILPDA, despite allegedly being a much weaker ATGL inhibitor than G0S2, have such a marked influence on lipid storage in macrophages? We hypothesize that HILPDA may require an interaction with an auxiliary factor for full activity. Further research is necessary to identify the mechanism for the differential potency of HILPDA in cell-free systems compared with live cells. Second, what is the reason for having two related ATGL inhibitors? Although our preliminary data suggest that in BMDMs, HILPDA is much more abundant than G0S2; it seems that in certain cells, such as cultured hepatocytes, HILPDA and G0S2 co-exist. Inasmuch as HILPDA and G0S2 are induced by different stimuli, they may be active under different circumstances. So far, there is no evidence for any functional dependency between the two proteins. Further research is necessary to better characterize the relationship and relative roles of these two homologous proteins in different cell types.

In conclusion, our data demonstrate that HILPDA is a lipid-inducible, physiological inhibitor of ATGL-mediated lipolysis in macrophages. In obese mice, HILPDA uncouples lipid droplet accumulation in adipose tissue macrophages from inflammation and metabolic dysregulation. Overall, our data question the importance of lipid storage in adipose tissue macrophages in obesity-induced inflammation and metabolic dysregulation.

STAR★METHODS

Detailed methods are provided in the online version of this paper and include the following:

SUPPLEMENTAL INFORMATION

Supplemental Information can be found online at https://doi.org/10.1016/j.celrep.2020.01.046.

ACKNOWLEDGMENTS

We would like to thank Shohreh Keshtkar, Karin Mudde, Jenny Jansen, Anneke Hijmans, Tessa de Bie, and Jacqueline Ratter for their technical assistance. This work was financed by grants from the Netherlands Organisation of Scientific Research (2014/12393/ALW), the Dutch Diabetes Foundation (2015.82.1824), and the Netherlands Heart Foundation (ENERGISE grant CVON2014-02).

AUTHOR CONTRIBUTIONS

X.A.M.H.v.D., M.A.d.l.R, A.G., F.M., W.D., J.W.B., R. Stienstra, and S.K. conceived and planned the research and experiments. X.A.M.H.v.D. carried out the *Hilpda*$^{\Delta M\Phi}$ mouse studies. X.A.M.H.v.D., M.A.d.l.R., A.G., F.M., and W.D. performed the experiments and analyzed the data. M.v.W. performed the lipidomics analysis. R. Singh, and J.W.B. contributed to the interpretation of the results. X.A.M.H.v.D. performed the statistical analyses. X.A.M.H.v.D., R. Stienstra, and S.K. wrote the manuscript. All authors provided critical feedback and helped to shape the research, analysis, and manuscript. Co-first author order was determined by contribution.

DECLARATION OF INTERESTS

The authors declare no competing interests.

Received: July 18, 2019
Revised: December 10, 2019
Accepted: January 15, 2020
Published: February 11, 2020

REFERENCES

Aflaki, E., Balenga, N.A.B., Luschnig-Schratl, P., Wolinski, H., Povoden, S., Chandak, P.G., Bogner-Strauss, J.G., Eder, S., Konya, V., Kohlwein, S.D., et al. (2011a). Impaired Rho GTPase activation abrogates cell polarization

and migration in macrophages with defective lipolysis. Cell. Mol. Life Sci. *68*, 3933–3947.

Aflaki, E., Radović, B., Chandak, P.G., Kolb, D., Eisenberg, T., Ring, J., Fertschai, I., Uellen, A., Wolinski, H., Kohlwein, S.D., et al. (2011b). Triacylglycerol accumulation activates the mitochondrial apoptosis pathway in macrophages. J. Biol. Chem. *286*, 7418–7428.

Aflaki, E., Doddapattar, P., Radović, B., Povoden, S., Kolb, D., Vujić, N., Wegscheider, M., Koefeler, H., Hornemann, T., Graier, W.F., et al. (2012). C16 ceramide is crucial for triacylglycerol-induced apoptosis in macrophages. Cell Death Dis. *3*, e280.

Bolstad, B.M., Irizarry, R.A., Astrand, M., and Speed, T.P. (2003). A comparison of normalization methods for high density oligonucleotide array data based on variance and bias. Bioinformatics *19*, 185–193.

Boutens, L., and Stienstra, R. (2016). Adipose tissue macrophages: going off track during obesity. Diabetologia *59*, 879–894.

Chandak, P.G., Radović, B., Aflaki, E., Kolb, D., Buchebner, M., Fröhlich, E., Magnes, C., Sinner, F., Haemmerle, G., Zechner, R., et al. (2010). Efficient phagocytosis requires triacylglycerol hydrolysis by adipose triglyceride lipase. J. Biol. Chem. *285*, 20192–20201.

Cinti, S., Mitchell, G., Barbatelli, G., Murano, I., Ceresi, E., Faloia, E., Wang, S., Fortier, M., Greenberg, A.S., and Obin, M.S. (2005). Adipocyte death defines macrophage localization and function in adipose tissue of obese mice and humans. J. Lipid Res. *46*, 2347–2355.

Coats, B.R., Schoenfelt, K.Q., Barbosa-Lorenzi, V.C., Peris, E., Cui, C., Hoffman, A., Zhou, G., Fernandez, S., Zhai, L., Hall, B.A., et al. (2017). Metabolically activated adipose tissue macrophages perform detrimental and beneficial functions during diet-induced obesity. Cell Rep. *20*, 3149–3161.

Dai, M., Wang, P., Boyd, A.D., Kostov, G., Athey, B., Jones, E.G., Bunney, W.E., Myers, R.M., Speed, T.P., Akil, H., et al. (2005). Evolving gene/transcript definitions significantly alter the interpretation of GeneChip data. Nucleic Acids Res. *33*, e175.

Denko, N., Schindler, C., Koong, A., Laderoute, K., Green, C., and Giaccia, A. (2000). Epigenetic regulation of gene expression in cervical cancer cells by the tumor microenvironment. Clin. Cancer Res. *6*, 480–487.

Dijk, W., Mattijssen, F., de la Rosa Rodriguez, M., Loza Valdes, A., Loft, A., Mandrup, S., Kalkhoven, E., Qi, L., Borst, J.W., and Kersten, S. (2017). Hypoxia-inducible lipid droplet-associated is not a direct physiological regulator of lipolysis in adipose tissue. Endocrinology *158*, 1231–1251.

DiStefano, M.T., Danai, L.V., Roth Flach, R.J., Chawla, A., Pedersen, D.J., Guilherme, A., and Czech, M.P. (2015). The lipid droplet protein hypoxia-inducible gene 2 promotes hepatic triglyceride deposition by inhibiting lipolysis. J. Biol. Chem. *290*, 15175–15184.

DiStefano, M.T., Roth Flach, R.J., Senol-Cosar, O., Danai, L.V., Virbasius, J.V., Nicoloro, S.M., Straubhaar, J., Dagdeviren, S., Wabitsch, M., Gupta, O.T., et al. (2016). Adipocyte-specific hypoxia-inducible gene 2 promotes fat deposition and diet-induced insulin resistance. Mol. Metab. *5*, 1149–1161.

Gimm, T., Wiese, M., Teschemacher, B., Deggerich, A., Schödel, J., Knaup, K.X., Hackenbeck, T., Hellerbrand, C., Amann, K., Wiesener, M.S., et al. (2010). Hypoxia-inducible protein 2 is a novel lipid droplet protein and a specific target gene of hypoxia-inducible factor-1. FASEB J. *24*, 4443–4458.

Goeritzer, M., Schlager, S., Radovic, B., Madreiter, C.T., Rainer, S., Thomas, G., Lord, C.C., Sacks, J., Brown, A.L., Vujic, N., et al. (2014). Deletion of CGI-58 or adipose triglyceride lipase differently affects macrophage function and atherosclerosis. J. Lipid Res. *55*, 2562–2575.

Gregor, M.F., and Hotamisligil, G.S. (2011). Inflammatory mechanisms in obesity. Annu. Rev. Immunol. *29*, 415–445.

Haemmerle, G., Moustafa, T., Woelkart, G., Büttner, S., Schmidt, A., van de Weijer, T., Hesselink, M., Jaeger, D., Kienesberger, P.C., Zierler, K., et al. (2011). ATGL-mediated fat catabolism regulates cardiac mitochondrial function via PPAR-α and PGC-1. Nat. Med. *17*, 1076–1085.

Herzog, K., Pras-Raves, M.L., Vervaart, M.A.T., Luyf, A.C.M., van Kampen, A.H.C., Wanders, R.J.A., Waterham, H.R., and Vaz, F.M. (2016). Lipidomic analysis of fibroblasts from Zellweger spectrum disorder patients identifies disease-specific phospholipid ratios. J. Lipid Res. *57*, 1447–1454.

Hill, D.A., Lim, H.W., Kim, Y.H., Ho, W.Y., Foong, Y.H., Nelson, V.L., Nguyen, H.C.B., Chegireddy, K., Kim, J., Habertheuer, A., et al. (2018). Distinct macrophage populations direct inflammatory versus physiological changes in adipose tissue. Proc. Natl. Acad. Sci. USA *115*, E5096–E5105.

Hotamisligil, G.S. (2017). Inflammation, metaflammation and immunometabolic disorders. Nature *542*, 177–185.

Huang, S.C.C., Everts, B., Ivanova, Y., O'Sullivan, D., Nascimento, M., Smith, A.M., Beatty, W., Love-Gregory, L., Lam, W.Y., O'Neill, C.M., et al. (2014). Cell-intrinsic lysosomal lipolysis is essential for alternative activation of macrophages. Nat. Immunol. *15*, 846–855.

Irizarry, R.A., Bolstad, B.M., Collin, F., Cope, L.M., Hobbs, B., and Speed, T.P. (2003). Summaries of Affymetrix GeneChip probe level data. Nucleic Acids Res. *31*, e15.

Jung, S.B., Choi, M.J., Ryu, D., Yi, H.S., Lee, S.E., Chang, J.Y., Chung, H.K., Kim, Y.K., Kang, S.G., Lee, J.H., et al. (2018). Reduced oxidative capacity in macrophages results in systemic insulin resistance. Nat. Commun. *9*, 1551.

Kratz, M., Coats, B.R., Hisert, K.B., Hagman, D., Mutskov, V., Peris, E., Schoenfelt, K.Q., Kuzma, J.N., Larson, I., Billing, P.S., et al. (2014). Metabolic dysfunction drives a mechanistically distinct proinflammatory phenotype in adipose tissue macrophages. Cell Metab. *20*, 614–625.

Lumeng, C.N., Bodzin, J.L., and Saltiel, A.R. (2007). Obesity induces a phenotypic switch in adipose tissue macrophage polarization. J. Clin. Invest. *117*, 175–184.

Lumeng, C.N., DelProposto, J.B., Westcott, D.J., and Saltiel, A.R. (2008). Phenotypic switching of adipose tissue macrophages with obesity is generated by spatiotemporal differences in macrophage subtypes. Diabetes *57*, 3239–3246.

Maier, A., Wu, H., Cordasic, N., Oefner, P., Dietel, B., Thiele, C., Weidemann, A., Eckardt, K.U., and Warnecke, C. (2017). Hypoxia-inducible protein 2 Hig2/Hilpda mediates neutral lipid accumulation in macrophages and contributes to atherosclerosis in apolipoprotein E-deficient mice. FASEB J. *31*, 4971–4984.

Mattijssen, F., Georgiadi, A., Andasarie, T., Szalowska, E., Zota, A., Krones-Herzig, A., Heier, C., Ratman, D., De Bosscher, K., Qi, L., et al. (2014). Hypoxia-inducible lipid droplet-associated (HILPDA) is a novel peroxisome proliferator-activated receptor (PPAR) target involved in hepatic triglyceride secretion. J. Biol. Chem. *289*, 19279–19293.

Mayer, N., Schweiger, M., Romauch, M., Grabner, G.F., Eichmann, T.O., Fuchs, E., Ivkovic, J., Heier, C., Mrak, I., Lass, A., et al. (2013). Development of small-molecule inhibitors targeting adipose triglyceride lipase. Nat. Chem. Biol. *9*, 785–787.

Namgaladze, D., and Brüne, B. (2016). Macrophage fatty acid oxidation and its roles in macrophage polarization and fatty acid-induced inflammation. Biochim. Biophys. Acta *1861*, 1796–1807.

Ong, K.T., Mashek, M.T., Bu, S.Y., Greenberg, A.S., and Mashek, D.G. (2011). Adipose triglyceride lipase is a major hepatic lipase that regulates triacylglycerol turnover and fatty acid signaling and partitioning. Hepatology *53*, 116–126.

Oteng, A.B., Ruppert, P.M.M., Boutens, L., Dijk, W., van Dierendonck, X.A.M.H., Olivecrona, G., Stienstra, R., and Kersten, S. (2019). Characterization of ANGPTL4 function in macrophages and adipocytes using *Angptl4*-knockout and *Angptl4*-hypomorphic mice. J. Lipid Res. *60*, 1741–1754.

Padmanabha Das, K.M., Wechselberger, L., Liziczai, M., De la Rosa Rodriguez, M., Grabner, G.F., Heier, C., Viertlmayr, R., Radler, C., Lichtenegger, J., Zimmermann, R., et al. (2018). Hypoxia-inducible lipid droplet-associated protein inhibits adipose triglyceride lipase. J. Lipid Res. *59*, 531–541.

Prieur, X., Mok, C.Y.L., Velagapudi, V.R., Núñez, V., Fuentes, L., Montaner, D., Ishikawa, K., Camacho, A., Barbarroja, N., O'Rahilly, S., et al. (2011). Differential lipid partitioning between adipocytes and tissue macrophages modulates macrophage lipotoxicity and M2/M1 polarization in obese mice. Diabetes *60*, 797–809.

Rausch, M.E., Weisberg, S., Vardhana, P., and Tortoriello, D.V. (2008). Obesity in C57BL/6J mice is characterized by adipose tissue hypoxia and cytotoxic T-cell infiltration. Int. J. Obes. *32*, 451–463.

Reid, B.N., Ables, G.P., Otlivanchik, O.A., Schoiswohl, G., Zechner, R., Blaner, W.S., Goldberg, I.J., Schwabe, R.F., Chua, S.C., Jr., and Huang, L.S. (2008). Hepatic overexpression of hormone-sensitive lipase and adipose triglyceride lipase promotes fatty acid oxidation, stimulates direct release of free fatty acids, and ameliorates steatosis. J. Biol. Chem. *283*, 13087–13099.

Robblee, M.M., Kim, C.C., Porter Abate, J., Valdearcos, M., Sandlund, K.L.M., Shenoy, M.K., Volmer, R., Iwawaki, T., and Koliwad, S.K. (2016). Saturated fatty acids engage an IRE1α-dependent pathway to activate the NLRP3 inflammasome in myeloid cells. Cell Rep. *14*, 2611–2623.

Rueden, C.T., Schindelin, J., Hiner, M.C., DeZonia, B.E., Walter, A.E., Arena, E.T., and Eliceiri, K.W. (2017). ImageJ2: ImageJ for the next generation of scientific image data. BMC Bioinformatics *18*, 529.

Sapiro, J.M., Mashek, M.T., Greenberg, A.S., and Mashek, D.G. (2009). Hepatic triacylglycerol hydrolysis regulates peroxisome proliferator-activated receptor α activity. J. Lipid Res. *50*, 1621–1629.

Saraswathi, V., and Hasty, A.H. (2009). Inhibition of long-chain acyl coenzyme A synthetases during fatty acid loading induces lipotoxicity in macrophages. Arterioscler. Thromb. Vasc. Biol. *29*, 1937–1943.

Sathyanarayan, A., Mashek, M.T., and Mashek, D.G. (2017). ATGL promotes autophagy/lipophagy via SIRT1 to control hepatic lipid droplet catabolism. Cell Rep. *19*, 1–9.

Schindelin, J., Arganda-Carreras, I., Frise, E., Kaynig, V., Longair, M., Pietzsch, T., Preibisch, S., Rueden, C., Saalfeld, S., Schmid, B., et al. (2012). Fiji: an open-source platform for biological-image analysis. Nat. Methods *9*, 676–682.

Schlager, S., Goeritzer, M., Jandl, K., Frei, R., Vujic, N., Kolb, D., Strohmaier, H., Dorow, J., Eichmann, T.O., Rosenberger, A., et al. (2015). Adipose triglyceride lipase acts on neutrophil lipid droplets to regulate substrate availability for lipid mediator synthesis. J. Leukoc. Biol. *98*, 837–850.

Shapiro, H., Pecht, T., Shaco-Levy, R., Harman-Boehm, I., Kirshtein, B., Kuperman, Y., Chen, A., Blüher, M., Shai, I., and Rudich, A. (2013). Adipose tissue foam cells are present in human obesity. J. Clin. Endocrinol. Metab. *98*, 1173–1181.

Van den Bossche, J., Baardman, J., Otto, N.A., van der Velden, S., Neele, A.E., van den Berg, S.M., Luque-Martin, R., Chen, H.J., Boshuizen, M.C.S., Ahmed, M., et al. (2016). Mitochondrial dysfunction prevents repolarization of inflammatory macrophages. Cell Rep. *17*, 684–696.

Xu, X., Grijalva, A., Skowronski, A., van Eijk, M., Serlie, M.J., and Ferrante, A.W., Jr. (2013). Obesity activates a program of lysosomal-dependent lipid metabolism in adipose tissue macrophages independently of classic activation. Cell Metab. *18*, 816–830.

Yang, X., Lu, X., Lombès, M., Rha, G.B., Chi, Y.I., Guerin, T.M., Smart, E.J., and Liu, J. (2010). The G(0)/G(1) switch gene 2 regulates adipose lipolysis through association with adipose triglyceride lipase. Cell Metab. *11*, 194–205.

Zhang, X., Saarinen, A.M., Hitosugi, T., Wang, Z., Wang, L., Ho, T.H., and Liu, J. (2017). Inhibition of intracellular lipolysis promotes human cancer cell adaptation to hypoxia. eLife *6*, e31132.

STAR★METHODS

KEY RESOURCES TABLE

REAGENT or RESOURCE	SOURCE	IDENTIFIER
Antibodies		
CD45-ECD anti-mouse	Beckman Coulter	Cat# A07784
F4/80-FITC anti-mouse	BioLegend	Cat# 123107; RRID: AB_893500
CD206-APC anti-mouse	BioLegend	Cat# 141707; RRID: AB_10896057
CD11c-PE-Cy7 anti-mouse	BioLegend	Cat# 117317; RRID: AB_493569
CD11b-PE anti-mouse	BioLegend	Cat# 101207; RRID: AB_312790
F4/80 anti-mouse	Bio-Rad	Cat# MCA497G; RRID: AB_872005
CD68 anti-mouse	AbD Serotec, Bio-Rad	Cat# MCA1957; RRID: AB_322219
HILPDA (HIG2, C-14) anti-mouse	Santa Cruz, Biotechnology	Cat# sc-137518; RRID: AB_2011522
ATGL	Santa Cruz Biotechnology	Cat# sc-365278, RRID:AB_10859044
PLIN3 (TIP47, M6PRBP1)	Proteintech	Cat# 10694-1-AP, RRID:AB_2297252
G0S2	Santa Cruz Biotechnology	Cat# sc-133424; RRID:AB_2107211
ACTIN	Cell Signaling	Cat# 5057; RRID: AB_10694076
TUBULIN	Cell Signaling	Cat# 2146; RRID: AB_2210545
HSP90	Cell Signaling	Cat# 4874S; RRID: AB_2121214
F4/80-FITC anti-mouse for MACS	Miltenyi Biotec	Cat# 130-117-509; RRID: AB_2727970
Anti-FITC microbeads	Miltenyi Biotec	Cat# 130-048-701; RRID: AB_244371
Bacterial and Virus Strains		
Ad-m-2310016C08RIK (AV-*Hilpda*)	Vector Biolabs	Cat# ADV-250639
Ad-GFP	Vector Biolabs	Cat# 1060
Chemicals, Peptides, and Recombinant Proteins		
Atglistatin	Sigma-Aldrich	Cat# SML1075
BODIPY® 493-503	ThermoFisher Scientific	Cat# D3922; CAS: 121207-31-6
BODIPY-FL® C12	ThermoFisher Scientific	Cat# D3822
2,2′-bipyridyl	Sigma-Aldrich	Cat# D216305; CAS: 366-18-7
Critical Commercial Assays		
GeneChip Whole-Transcript Sense Target Assay kit	Affymetrix	Cat# P/N900652
QBT Fatty Acid Uptake Assay Kit	Molecular Devices	Cat# R6132
IL6 DuoSet Sandwich ELISA	R&D Systems	Cat# DY406
TNFα DuoSet Sandwich ELISA	R&D Systems	Cat# DY410
IL10 DuoSet Sandwich ELISA	R&D Systems	Cat# DY417
Deposited Data		
Microarray dataset peritoneal macrophages treated with fatty acids	This paper	GEO: GSE142296
Microarray dataset: peritoneal macrophages treated with intralipid	Oteng et al., 2019	GEO: GSE136240
Microarray dataset: Hilpda$^{\Delta M\Phi}$ and Hilpda$^{flox/flox}$ BMDMs treated with oleate:palmitate	This paper	GEO: GSE142296
Microarray dataset: WT BMDMs treated fatty acids or LPS	Robblee et al., 2016	GEO: GSE77104
Microarray dataset: adipose tissue macrophages	Boutens and Stienstra, 2016	GEO: GSE84000

(*Continued on next page*)

Continued		
REAGENT or RESOURCE	SOURCE	IDENTIFIER
Experimental Models: Cell Lines		
RAW264.7 authenticated murine macrophage cell line	Sigma-Aldrich	Cat#91062702; RRID: CVCL_0493
Experimental Models: Organisms/Strains		
Mouse: Hilpda$^{tm1.1Nat}$/J	Jackson Laboratories	JAX: 017360; RRID: MGI:5285399
Mouse: B6.129P2-$^{Lyz2tm1(cre)Ifo}$/J	Jackson Laboratories	JAX: 004781; RRID: IMSR_JAX:004781
Oligonucleotides		
Primers for RT-PCR, see Table S1	This paper	N/A
Software and Algorithms		
Fiji	Schindelin et al., 2012, Rueden et al., 2017	https://fiji.sc/
Kaluza	Beckman Coulter	RRID: SCR_016182
Seahorse XF-96 Wave	Agilent Technologies	RRID: SCR_014526
CRAN for R programming language	http://cran.r-project.org/	CRAN; RRID: SCR_003005
Other		
Palmitic acid	Sigma-Aldrich	Cat# P0500; CAS: 57-10-3
Oleic acid	Sigma-Aldrich	Cat# O1008; CAS: 112-80-1
Intralipid	Baxter	Cat# 0338-0519-58
Collagenase from *Clostridium histolyticum*	Sigma-Aldrich	Cat# C6885; CAS: 9001-12-1
Standardized rodent high-fat diet	Research Diets	Cat# D12451
Standardized rodent low-fat diet	Research Diets	Cat# D12450H

LEAD CONTACT AND MATERIALS AVAILABILITY

Further information and requests for resources should be directed to and will be fulfilled by the Lead Contact, Sander Kersten (sander.kersten@wur.nl). This study did not generate new unique reagents.

EXPERIMENTAL MODEL AND SUBJECT DETAILS

Animal Studies

Studies were performed using purebred wild-type C57BL/6 mice, *Hilpda*$^{\Delta M\Phi}$ mice and their *Hilpda*$^{flox/flox}$ littermates. *Hilpda*$^{flox/flox}$ were acquired (Jackson Laboratories, Bar Harbor, ME; Hilpda$^{tm1.1Nat}$/J, JAX: #017360, RRID: MGI:5285399) and backcrossed onto a C57BL/6 background in our facility for at least 5 generations. LysM-Cre transgenic mice (B6.129P2-$^{Lyz2tm1(cre)Ifo}$/J, JAX:#004781, RRID: IMSR_JAX:004781) were acquired from Jackson laboratories. Prior to arrival at Jackson laboratories, the lysM-Cre transgenic mice have been backcrossed onto a C57BL/6 background for at least six generations. In our facility, the *Hilpda*$^{flox/flox}$ were crossed with *lysM*-Cre transgenic mice to generate mice with a mature myeloid cell-specific Cre-mediated deletion of *Hilpda* on a C57BL/6 background. The identity of the C57BL/6 background strain was not confirmed by sequencing. Mice were individually housed under normal light-dark cycles in temperature- and humidity-controlled specific pathogen-free conditions. Mice had *ad libitum* access to food and water. The experimenter was blinded to group assignments during all analyses. For *in vivo* studies, male mice were used with an age of 9-12 weeks. For the isolation of primary cell cultures, both male and female mice were used with an age of 8-12 weeks. All animal experiments were approved by the local animal welfare committee of Wageningen University (AVD104002015236, 2016.W-0093.001).

Cell Lines and Primary Cultures

RAW264.7 macrophage cells (Cat#91062702; RRID: CVCL_0493, Sigma-Aldrich, Darmstadt, Germany) and bone-marrow derived macrophages were cultured in Dulbecco's modified Eagle's medium (DMEM, Corning, NY, USA), supplemented with 1% penicillin/streptomycin (P/S, Corning). Adipose tissue macrophages and peritoneal macrophages were cultured in Roswell Park Memorial Institute (RPMI)-1630 medium (Lonza, Basel, Zwitserland) supplemented with 10% FCS and 1% P/S. All cells were kept in incubators at 37°C/5% CO_2. Primary cell cultures were isolated from male and female wild-type C57BL/6, *Hilpda*$^{\Delta M\Phi}$ and *Hilpda*$^{flox/flox}$ mice aged 8-12 weeks. RAW264.7 macrophages were purchased as authenticated cell line from Sigma-Aldrich.

METHOD DETAILS

Mouse Studies

Per genotype, 12 male *Hilpda*$^{\Delta M\Phi}$ mice aged 9-12 weeks or their male *Hilpda*$^{flox/flox}$ littermates were randomly allocated using an online randomization tool to either a standardized high fat diet or a low fat diet (formula D12451 and formula D12450H respectively, Research Diets, New Brunswick, USA; γ-irradiated with 10-20 kGy) for 20 weeks. Body weight and feed intake were assessed weekly. At the end of the study, mice were anaesthetised with isoflurane and blood was collected via orbital puncture in tubes containing EDTA (Sarstedt, Nümbrecht, Germany). Subsequently, mice were immediately euthanized by cervical dislocation, after which tissues were excised, weighed and frozen in liquid nitrogen or prepared for histology. Frozen samples were stored at -80°C.

Intraperitoneal Glucose Tolerance Test

In the HFD-LFD study, an intraperitoneal glucose tolerance test was performed after 18 weeks. Mice were fasted for 5 hours and blood was collected via tail bleeding at 0, 15, 30, 45, 60, 90 and 120 minutes after i.p. injection of 1g/kg bodyweight glucose (Baxter, Deerfield, IL, USA). Blood glucose was measured with a GLUCOFIX Tech glucometer and glucose sensor test strips (GLUCOFIX Tech, Menarini Diagnostics, Valkenswaard, the Netherlands). A time point of 150 minutes after injection of glucose was added for the high fat diet fed groups.

Plasma Measurements

Blood collected in EDTA tubes was spun down for 15 minutes at 5000 RPM at 4°C. Plasma was aliquoted and stored at -80°C until measurement of cholesterol (Liquicolor, Human GmbH, Wiesbaden, Germany), triglycerides (Liquicolor), glucose (Liquicolor), NEFAs (NEFA-HR set R1, R2 and standard, WAKO Diagnostics, Instruchemie, Delfzijl, the Netherlands), adiponectin (ELISA duoset kit, R&D Systems, Bio-techne, MN, USA), leptin (ELISA duoset kit, R&D Systems) and insulin (ultra-sensitive mouse insulin ELISA kit, Crystal Chem Inc., IL, USA) following manufacturer's instructions.

gWAT Explants and Adipose Macrophage Isolation

For SVF, adipocytes and adipose tissue macrophages isolation, gonadal adipose tissue (gWAT) was collected and kept in with DMEM supplemented with 1% P/S and 1% FFA-free Bovine Serum Albumin (BSA fraction V, Roche via Merck, Darmstadt, Germany) on ice. gWAT explants were taken into culture for 24h in DMEM, supplemented with 10% fetal calf serum (FCS, BioWest, Nuaillé, France) and 1% P/S. Supernatant was stored for ELISA measurements or as conditioned medium. For high fat diet groups, the stromal vascular fractions were isolated by digesting gWAT for 45 minutes in Roswell Park Memorial Institute (RPMI)-1630 medium (Lonza, Basel, Zwitserland) supplemented with 10% FCS, 1% P/S, 0.5% FFA-free BSA, 1M CaCl2, 1M HEPES and 0.15% collagenase (from Clostridium histolyticum, Sigma-Aldrich, Cat#C6885; CAS: 9001-12-1). Per three mice of the same group, gWAT was pooled after digestion, filtered through a 100μm cell strainer and centrifuged at 200 g for 10 min. Floating mature adipocytes were removed and stored separately and stromal vascular pellet was resuspended in erythrocyte lysis buffer and subsequently washed twice in phosphate buffered saline (PBS, Corning) supplemented with 0.5% FFA-free BSA and 2mM EDTA. Resulting stromal vascular fractions were used to isolate ATMs using mouse anti-F4/80-FITC antibodies (Cat#130-117-509; RRID: AB_2727970, Miltenyi Biotec, Bergisch Gladbach, Germany), anti-FITC MicroBeads (Cat#130-048-701; RRID: AB_244371, Miltenyi Biotec) and MS columns (Miltenyi Biotec) on an OctoMACS Cell Separator system (Miltenyi Biotec). ATMs were cultured for 24h in RPMI-1630 supplemented with 10% FCS and 1% P/S. ATMs were either cultured for 2h after which cells were washed with PBS, fixed in 3.7% paraformaldehyde and stained with Oil red O following standard protocols, or were cultured for 24h to obtain supernatants.

Flow Cytometry of SVF

Before isolation of ATMs, SVF pools were resuspended in PBS containing 0.5% BSA and 2mM EDTA and 500 000 cells were sampled and stained with antibodies against CD45-ECD (Cat#A07784, Beckman Coulter, Brea, CA, USA), F4/80-FITC (Cat#123107; RRID: AB_893500), CD206-APC (Cat#141707; RRID: AB_10896057), CD11c-PE-Cy7 (Cat#117317; RRID: AB_493569) and CD11b-PE (Cat#101207; RRID: AB_312790, Biolegend, San Diego, CA, USA). Samples were measured on a flow cytometer (FC500, Beckman Coulter) and results were analyzed using Kaluza analysis software 2.1 (RRID: SCR_016182, Beckman Coulter).

Histological Studies

Samples of gWAT for histological analysis were fixed in 3.7% paraformaldehyde immediately upon collection, embedded in paraffin, sectioned and stained with hematoxylin eosin according to standard protocols. After preincubation with 20% normal goat serum, paraffin-embedded sections were incubated at 4°C overnight with antibodies for F4/80 (Cat#MCA497G; RRID: AB_872005, Bio-Rad Laboratories, Hercules, CA, USA), HILPDA (sc-137518 HIG2 Antibody (C-14); RRID: AB_2011522, Santa-Cruz Biotechnology, Dallas, TX, USA Biotechnology) or CD68 (Cat#MCA1957; RRID: AB_322219, AbD Serotec, Bio-Rad Laboratories) dissolved in PBS supplemented with 1% BSA (Merck). Anti-rat or anti-rabbit IgG conjugated to HRP (Cell Signaling Technology, Danvers, MA, USA) were used as secondary antibody. Negative controls were prepared without using primary antibody.

Peritoneal Macrophages and BMDMs

To harvest peritoneal macrophages, 8-12 week old WT C57BL/6 mice were injected intraperitoneally with 1mL 4% thioglycolic acid. Three days post-injection, mice were anesthetised with isoflurane and euthanized by CO_2. Peritoneal cells were harvested by washing the peritoneal cavity with ice-cold RPMI-1630 supplemented with 10% heat-inactivated FCS (BioWest) and 1% P/S. Cells were plated after lysis of erythrocytes and non-adherent cells were washed away three hours post plating. To isolate BMDMs, 8-12 week old *Hilpda*$^{\Delta M\Phi}$ mice and their *Hilpda*$^{flox/flox}$ littermates were euthanized by cervical dislocation. Both femurs and hind legs were isolated at the hip joint, keeping femur and tibia intact. Bone marrow was extracted from the femur and tibia and differentiated in DMEM, supplemented with 10% FCS, 1% P/S and 15% L929 conditioned medium. After seven days of differentiation, BMDMs were scraped and plated as appropriate.

Cell Culture Experiments

RAW 264.7 macrophage cells (Cat#91062702; RRID: CVCL_0493, Sigma-Aldrich) were cultured in DMEM supplemented with 10% FCS and 1% P/S. Overexpression of *Hilpda* was achieved by transfection with an adenoviral construct containing either *Hilpda* (Ad-m-2310016C08RIK, ADV-250639, Vector Biolabs, Malvern, USA) or GFP (Ad-GFP, Cat#1060, Vector Biolabs, Malvern, USA) in a dose of 500 MOI for 48 hours. Palmitate (Cat#P0500; CAS: 57-10-3, Sigma-Aldrich) and oleate (Cat#O1008; CAS: 112-80-1, Sigma-Aldrich) were solubilized using EtOH and KOH and conjugated to FFA-free BSA in sterile water (Versol, Aguettant, Lyon, France) at 37°C for 30 min. Palmitate was used in concentrations of 200, 250 or 500μM. Oleate was used in a concentration of 250μM or 400μM together with 20 μM BODIPY-FL C12 (Cat#D3822, ThermoFisher Scientific, MA, USA) for fatty acid trafficking experiments. A mixture of oleate and palmitate (oleate:palmitate) was made in a ratio of 1:2 and used in a final concentration of 600 μM. Intralipid (Fresenius Kabi AB, Uppsala, Sweden) was used in a concentration of 1 or 2mM. The addition of 100μM iron chelator 2,2′-bipyridyl (Cat#D216305; CAS: 366-18-7, Sigma-Aldrich) was used to chemically mimic hypoxia. Atglistatin (Cat#SML1075, Sigma-Aldrich) was used in a concentration of 20μM in 100% DMSO and cells were pre-treated for 2 hours before fatty acid loading. 24 hour treatments containing Atglistatin were refreshed every 12 hours. All cells were washed with PBS (Corning) after treatment. BMDMs were stained with Oil Red O following standard procedures.

Confocal Imaging

To visualize fatty acid uptake, accumulation and trafficking, BMDMs were plated on 8-well μ glass bottom slides (Ibidi, Martinsried, Germany). Confocal imaging was performed on a Leica confocal TCS SP8 X system equipped with a 63 × 1.20 NA water-immersion objective lens. Images were acquired using 1,024 × 1,024 pixels with pinhole set at 1 Airy Unit (AU). Excitation of the fluorescent probes used in this study was performed using white light laser (WLL, 50% laser output) selecting the 488 nm laser line. Fluorescence emission was detected using internal Hybrid (HyD) detector selecting a spectral window from either 520 - 580 nm (fatty acid uptake) or from 510 – 565 nm (fatty acid trafficking).

Fatty acid uptake was measured on paraformaldehyde fixed cells after 35 minutes incubation with the QBT Fatty acid uptake assay kit (Cat#R6132, Molecular Devices, California, USA) according to manufacturer's instructions. Image analysis was performed with Fiji (https://fiji.sc/) (Schindelin et al., 2012; Rueden et al., 2017). Pixels were selected for analysis using Otsu threshold, mean intensity was quantified. The WLL laser line (488 nm) was set at a laser power of 0.2%. The pinhole was adjusted at 5.7 AU for fluorescence intensity measurements, whereas confocal imaging was done with a pinhole of 1 AU.

Fatty acid trafficking was assessed after lipid loading for 5h and 24h with 400 μM oleate and 20 μM BODIPY® FL C12, treated either with vehicle or Atglistatin. The WLL laser line (488 nm) was set at a laser power of 1.6% for 5 h incubated cells and 0.3% for 24 h incubated cells. Cells were washed with PBS, fixed for 15 min with 3.7% formaldehyde and mounted with Vectashield-H (Vector Laboratories, Peterborough, UK). Fire LUT was applied using Fiji.

To assess fatty acid accumulation, BMDMs treated with oleate:palmitate were washed with PBS and fixed for 15 minutes with 3.7% paraformaldehyde. Fixed cells were stained with 2μg/mL BODIPY® 493/503 (Thermo Fisher Scientific) and mounted with Vectashield-H (Vector Laboratories). Images were processed and analyzed with Fiji. Briefly, images were converted to binary, watershed and LD size and number was measured with particle analysis set 0.07 μm^2-infinity.

Extracellular Flux Assay

Extracellular flux of lipid-loaded BMDMs was measured using the Agilent Seahorse XF96 Analyzer (Agilent Technologies, Santa Clara, CA, USA). Cells were seeded in a density of 200 000 cells per well in XF-96 plates (Agilent Technologies), treated appropriately and kept in a 37°C/5% CO_2 incubator. An hour before the measurement, cells were washed and cultured in Seahorse XF base medium (Agilent Technologies) without sodium bicarbonate, supplemented with 25mM glucose and 2mM L-glutamine for one hour at 37°C in a non-CO_2 incubator. For the mitochondrial stress test, the following compounds were added during four injections: oligomycin (1.5μM), FCCP (1.5 μM), pyruvate (1mM), antimycin A (2.5 μM) and rotenone (1.25 μM). The oxygen consumption rate (OCR) was automatically measured by the sensor cartridge at baseline and following injections. Calculations were made using the Seahorse XF-96 software Wave Desktop 2.6 (RRID: SCR_014526, Agilent Technologies).

Real-Time PCR

For cells, total RNA was isolated using TRIzol® Reagent (Invitrogen, ThermoFisher Scientific). For tissues, total RNA was isolated using the RNeasy Micro Kit (QIAGEN, Venlo, the Netherlands). cDNA was synthesized from 500ng RNA using the iScript cDNA kit (Bio-Rad Laboratories, Hercules, CA, USA) according to manufacturer's instructions. Real-time polymerase chain reaction (RT-PCR) was performed with the CFX96 or CFX384 Touch Real-Time detection system (Bio-Rad Laboratories), using a SensiMix (BioLine, London, UK) protocol for SYBR green reactions. Mouse 36b4 expression was used for normalization.

Immunoblotting

Cell or tissue protein lysates were separated by electrophoresis on pre-cast 4%–15% polyacrylamide gels and transferred onto nitrocellulose membranes using a Trans-Blot® Semi-Dry transfer cell (all purchased from Bio-Rad Laboratories), blocked in non-fat milk and incubated overnight at 4°C with primary antibody for HILPDA (Cat#sc-137518; RRID: AB_2011522, Santa Cruz Biotechnology), ATGL (Cat#sc-365278, RRID:AB_10859044, Santa Cruz Biotechnology), PLIN3 (Cat#10694-1-AP, RRID:AB_2297252, Proteintech), G0S2 (Cat#sc-518067, Santa Cruz Biotechnology), ACTIN (Cat#5057; RRID: AB_10694076, Cell Signaling Technology), TUBULIN (Cat#2146; RRID: AB_2210545, Cell Signaling Technology) or HSP90 (Cat#4874S; RRID: AB_2121214, Cell Signaling Technology). Membranes were incubated with secondary antibody (Anti-rabbit IgG, HRP-linked Antibody, 7074, Cell Signaling Technology) and developed using Clarity ECL substrate (Bio-Rad Laboratories). Images were captured with the ChemiDoc MP system (Bio-Rad Laboratories).

Enzyme-Linked Immunosorbent Assay (ELISA)

DuoSet sandwich ELISA kits for TNFα, IL10 and IL6 (Cat#DY410/Cat#DY417/Cat#DY406, R&D systems) were used to measure cytokine concentrations in cell or explant supernatant according to manufacturer's instructions. Data were normalized for the amount of adipose tissue macrophages by determining the concentration of DNA per well (Quant-iT dsDNA Assay Kit high sensitivity, Thermo Fisher Scientific) and normalized for gWAT explants to the weight per explant.

Lipidomics

Lipidomics analysis was performed as described (Herzog et al., 2016). The HPLC system consisted of an Ultimate 3000 binary HPLC pump, a vacuum degasser, a column temperature controller, and an auto sampler (Thermo Fisher Scientific). The column temperature was maintained at 25°C. The lipid extract was injected onto a ''normal phase column'' LiChrospher 2x250-mm silica-60 column, 5 μm particle diameter (Merck) and a ''reverse phase column'' Acquity UPLC HSS T3, 1.8 μm particle diameter (Waters, Milford, MA, USA). A Q Exactive Plus Orbitrap (Thermo Fisher Scientific) mass spectrometer was used in the negative and positive electrospray ionization mode. Nitrogen was used as the nebulizing gas. The spray voltage used was 2500 V, and the capillary temperature was 256°C. S-lens RF level: 50, auxiliary gas: 11, auxiliary temperature 300°C, sheath gas: 48, sweep cone gas: 2. In both the negative and positive ionization mode, mass spectra of the lipid species were obtained by continuous scanning from m/z 150 to m/z 2000 with a resolution of 280,000 full width at half maximum (FWHM). Data were analyzed and visualized using R programming language (CRAN, RRID: SCR_003005, https://www.r-project.org).

Microarray Analyses

Microarray analysis was performed on a several experiments: 1) Peritoneal macrophages treated with various fatty acids (500 μM) for 6 hours. 2) Peritoneal macrophages treated with intralipid (2mM) for 6 hours. 3) BMDM samples from *Hilpda*$^{\Delta M\Phi}$ mice and H*ilpda*$^{flox/flox}$ mice lipid loaded with oleate:palmitate (600μM) for 12 and 24 hours. RNA was isolated as described above and purified with the RNeasy Micro kit from QIAGEN. Integrity of the RNA was verified with RNA 6000 Nano chips using an Agilent 2100 bioanalyzer (Agilent Technologies). Purified RNA (100 ng per sample) was labeled with the Whole-Transcript Sense Target Assay kit (Affymetrix, Santa Clara, CA, USA; P/N 900652) and hybridized to an Affymetrix Mouse Gene 1.0 arrays or 2.1 ST array plate (Affymetrix). Hybridization, washing, and scanning were carried out on an Affymetrix GeneTitan platform according to the manufacturer's instructions.

Visualization

The 3D scatterplot of signal log ratio's (Figure 1A) was created using R programming language (https://www.r-project.org) and the R package ''plot3D.'' Heat-maps for the lipidomics were created using the package ''gplots'' and. The graphical abstract was created with BioRender.

QUANTIFICATION AND STATISTICAL ANALYSIS

Power Calculation

From earlier studies it is known that fasting glucose values of mice fed a high fat diet differs on average 3mM (+ 8 mM – 11mM) compared to mice fed a low fat diet. Differences in responses lead to a standard deviation around 2mM or higher. For the power

calculation, we used a one-way ANOVA with a significance level of 0.05 and a power of 90%, leading to an estimation of around n = 11 mice needed per group. To allow compensation for unforeseen circumstances or potential loss of mice during the study, n = 12 mice were included per group.

Statistical Analysis

Normalization of the arrays was performed with the Robust Multi-array Average method (Bolstad et al., 2003; Irizarry et al., 2003). Probe sets were redefined according to Dai et al. (2005) based on annotations provided by the Entrez Gene database. Data for the 3D scatterplot of signal log ratio's (Figure 1A) was created using R programming language (https://www.r-project.org). Partial least-squares regression analysis for the lipidomics data was performed using the R package ''mixOMICS.''

Details on statistical analyses are given in figure legends. In experiments where animals were included, *n* represents the number of animals used. For cell experiments, *n* represents the number of replications performed. Data are represented as means ± SD or SEM as indicated. Assumptions for statistical methods were tested and statistical analyses were carried out using an unpaired Student's t test or two-way ANOVA followed by Bonferroni's post hoc multiple comparisons test, if genotype and diet or genotype and treatment both were found significant (GraphPad Software, San Diego, CA, USA). A value of $p < 0.05$ was considered statistically significant.

DATA AND CODE AVAILABILITY

A publicly available dataset (GEO: GSE77104) was downloaded from Gene Expression Omnibus and further processed as described above to obtain individual gene expression data (Robblee et al., 2016). The microarray analysis of the adipose tissue macrophages (GEO: GSE84000) and peritoneal macrophages treated with intralipid (GEO: GSE136240) are already described elsewhere (Boutens and Stienstra, 2016; Oteng et al., 2019). The accession number for the microarray datasets reported in this paper is GEO: GSE142296.